Journal of Mechanics and Solids

Volume No. 12

Issue No. 1

January - April 2024

ENRICHED PUBLICATIONS PVT. LTD

S-9, IInd FLOOR, MLU POCKET,
MANISH ABHINAV PLAZA-II, ABOVE FEDERAL BANK,
PLOT NO-5, SECTOR-5, DWARKA, NEW DELHI, INDIA-110075,
PHONE: - + (91)-(11)-47026006

Journal of Mechanics and Solids

Aims and Scope

Journal of Mechanics and Solids publishes quality papers covering a broad area of mechanical engineering activities associated with the classical problems of structural analysis to mechanics of solids, fracture, and heat transfer, thermal effects in solids, optimum design methods, and numerical techniques. The submitted Manuscripts should report original and unpublished research results and follow the style of the journal. No length limitations for contributions are set, but only concisely written papers will be published.

Journal of Mechanics and Solids

Editorial Board

Journal of Mechanics and Solids

(Volume No. 12, Issue No. 1, Jan - Apr 2024)

Contents

Go-Kart Chassis Analysis: Design Methodology Integrating Revolutionary Safety Features

Aditya Natu[1], Dr. T. Moasunep Jamir[2]

[1]Production and Industrial Engineering, Mechanical Engineering Department, Delhi Technological University,

[2]Mechanical Engineering Department, Assistant Professor, Delhi Technological University, Delhi-42

Email: sunepbokdi@gmail.com

Corresponding Author; Tel: +91 9971931922, Email: nathu.aditya@gmail.com

A B S T R A C T

This paper entails the unique design and implementation of the racing Go-Kart Chassis, mainly focussing on the revolutionary safety features. The paper primarily explores the new design philosophy by placing the engine behind the driver with firewall as added protection. The details study and analysis for the static and dynamic performances as well as the ergonomic feasibility has been performed on the chassis assembly.

Keywords- Racing Go-kart, Chassis Design and Assembly, Solid Modelling, FEA, ANSYS

I. INTRODUCTION

The present paper entails to analyse and manufacture a racing go- kart mainly focussing on the revolutionary safety features. Figure. 1, shows the assembled model of the racing go- kart. The detail theoretical studies and the analysis for static and dynamic performances as well as the ergonomic feasibility has been performed on the chassis assembly.

Fig.1 Assembled Kart Model – Isometric

II. CHASSIS

Definition and Purpose

Chassis of any vehicle is defined as the internal framework of a vehicle which supports and positions various components of the vehicle.[2] Chassis of a go-kart plays a significant role in the jacking of the kart while the kart is cornering. In the absence of a differential in a kart, chassis frame plays following pivotal roles in the performance:

- It allows for lifting of the rear inside wheel of the kart while cornering by the virtue of its flexibility and relatively low torsional stiffness [6]. This can cause the kart to turn very smoothly even without a differential.
- It acts as a spring to absorb various shocks and vibrations from the road to provide maximum comfort to the driver

Design Objectives

The frame of the kart chassis was designed with following aims:

- To have minimum wheelbase and track-width and ergonomic norms to improve cornering performance.
- To weigh less than 20 kg.
- To be flexible enough to allow rear 'jacking' effect and absorb road shocks.
- To protect the driver in front and side crash events.
- To provide comfortable posture to a large range of driver statures
- To be easy to fabricate
- To have an open airflow over the engine compartment for cooling.
- Keeping the above mentioned objectives in view, a tubular double rail chassis was used in the front part to facilitate an open ergonomically suitable compartment.

Design Methodology

Fig. 2 shows the design workflow that was adopted for this project:

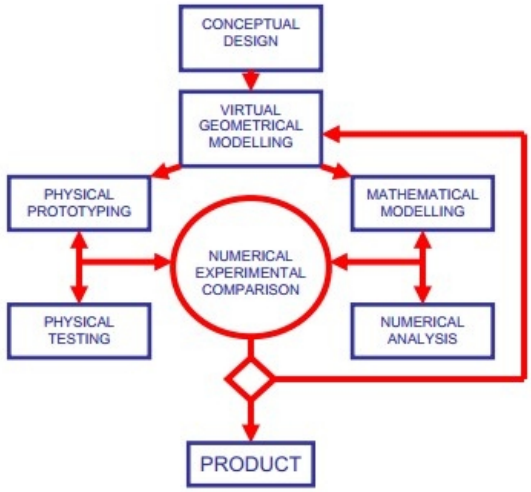

Fig.2 Design Methodology [1]

Conceptual design was initially agreed upon keeping all the initial design parameters in view.

Thereafter, virtual modelling was done on Solid Works 2014 for frame which was then analysed structurally by ANSYS Workbench 12.0. Using this software, greatly reduced the chances of error which easily creep up in FEA (Finite Element Analysis).

The model was further analysed in dynamic loading conditions in ANSYS for cornering performance etc. and ergonomic analysis was done in CATIA v5 R20. Changes were made in the design to satisfy all conditions necessary. Multi-body modelling was done to accommodate all the auxiliary components on the frame.

Chassis Specifications

Material Selection: Various parameters were kept in view while deciding the frame material which included availability, cost, machinability and tensile strength. Fig. 3 shows a plot of statistical data compiled for various materials that were analysed for kart frame. AISI 1020 was selected to be the frame material for:

- Low cost
- High weldability
- High availability
- Moderate Strength

Cross Section: The cross section for the members was chosen as circular tubular for its higher torsional stiffness for a given area of cross section compared to square and other sections. The standard cross section determined after market research was 25.4mm OD, 22mm ID.

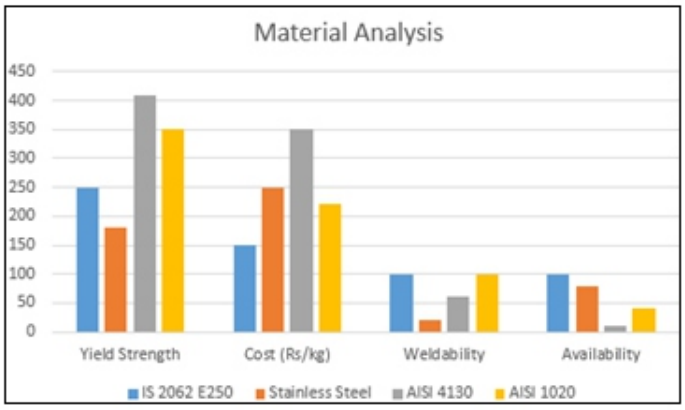

Fig.3 Material Analysis for kart strength [1]

Material Properties of AISI 1020 steel are given in the table below:

TABLE 1: MATERIAL PROPERTIES

Property	Value
Density	7.87g/cc
Elastic Modulus	200Gpa
Poisson's Ratio	0.290
Yield Strength	294.74Mpa
Ultimate Tensile Strength	394.72MPa

Final Chassis Layout: The three normal views of frame are shown in following figures:

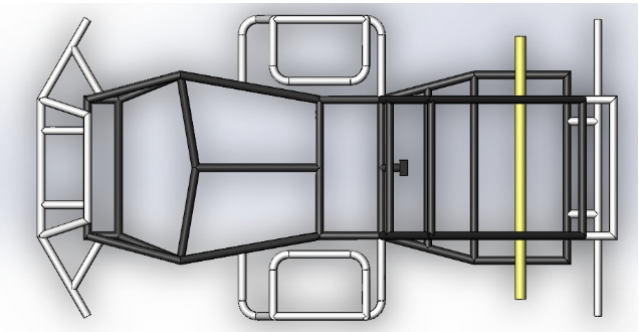

Fig. 4 Top View of Chassis

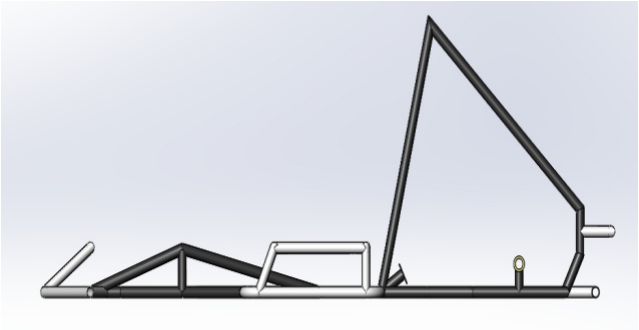

Fig. 5 Side View of Chassis

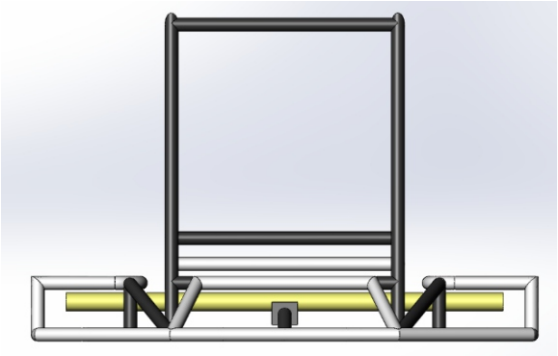

Fig. 6 Front View of Chassis

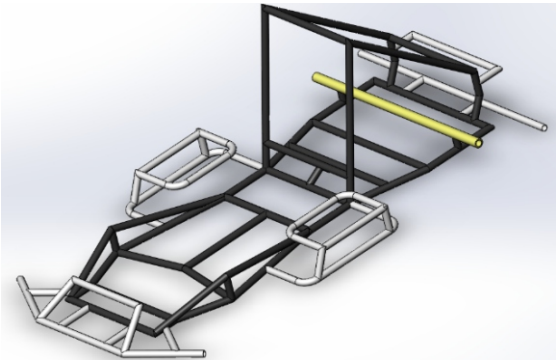

Fig. 7 Isometric View of Chassis

Final Geometrical Parameters: Major dimensions which associated with the frame have been tabulated in Table 2.

TABLE 2: FRAME PARAMETERS [3]

Parameter	**Value (mm)**
Wheelbase	1100mm
Front Track	850mm
Rear Track	850mm
Total Length	1860mm
Total Height	750mm
Total Width	1100mm
Cross Sectional Data	
Type	Tubular
Outer Diameter	25.4mm
Inner Diameter	22mm

Finite Element Analysis

FEA methodology: The finite element theory was employed for predicting the behaviour of chassis under the methods proposed in the Fig. 8.

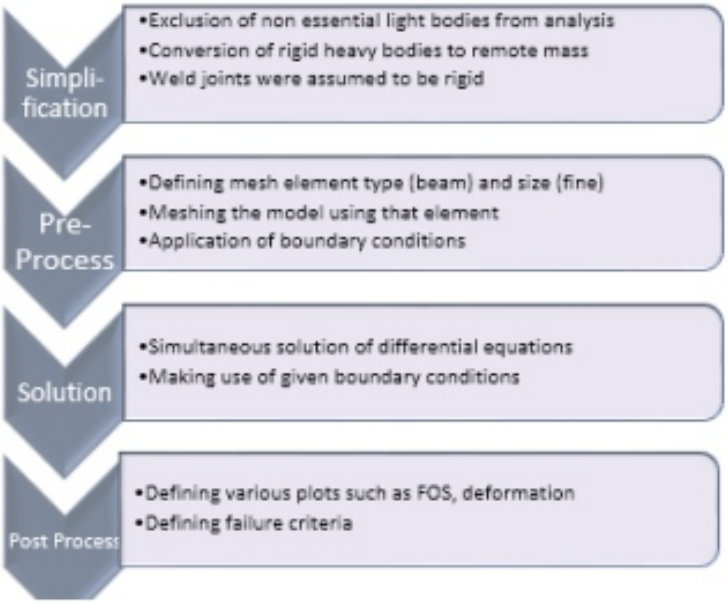

FEA is a method in which the model is discretized into small elements, properties of which are then evaluated using general equations of motion and boundary conditions specified during a test. This involves solution of the equation:

$$[\text{Reaction}] = [\text{Stiffness}] * [\text{Displacement}] + [\text{Load}]$$

The non-structural elements such as driver and engine were modelled as remote mass [5] acting on their respective mounting positions. Also, the analysis was done in ANSYS WB to get better validated results under same loaded conditions.

Grid Characteristics: The frame was meshed from beam elements for analysis.

In ANSYS WB, the model was generated automatically from beam elements with 6 degrees of freedom for every element.

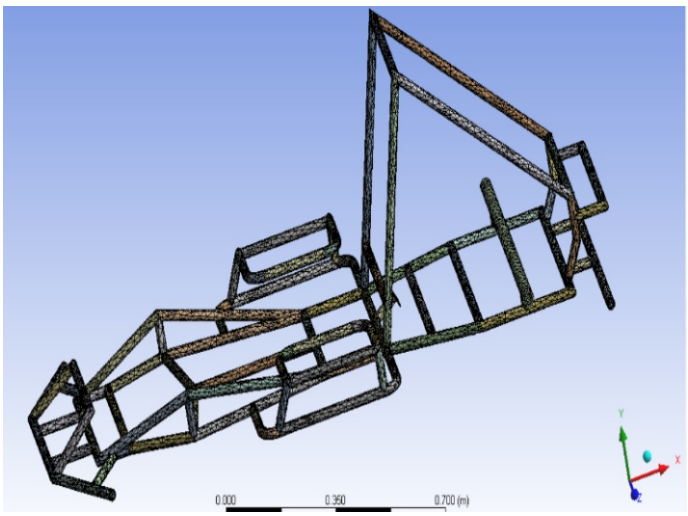

Fig 9. Beam mesh in ANSYS WB

The members which were predicted to be the heaviest loaded were applied 'fine' mesh control to gain better accuracy. The final mesh for ANSYS WB is shown in Fig. 9.

After setting the mesh, 5 static studies were performed on the model:

a) Static Bending Test
b) Torsional Stiffness Test
c) Front Impact Test
d) Side Impact Test

These models have been discussed in detail in the upcoming section.

Loading Diagram Abbreviations:-

- Red Arrows- Driver Weight (700N)
- Red Arrows- Engine Weight (250N)
- Red Arrows- Moment on axle (1000Nm)
- Red Arrows- Impact Forces
- Blue Tags- Fixed Supports
- Yellow Arrows- Gravity

Static Bending Test

In this test, various stresses developed in a fully loaded chassis were analysed.

TABLE 3: LOADING DIAGRAM

Loads	Driver, Engine gravity loads at mounting position
Constraints	Wheel Hub mounting positions
Gravity	On

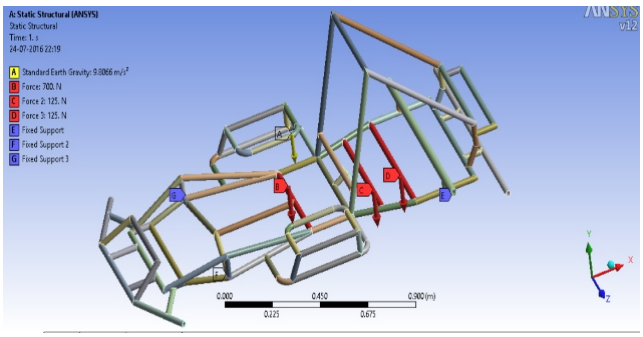

Fig. 10. Loading Diagram of Static Bending Test

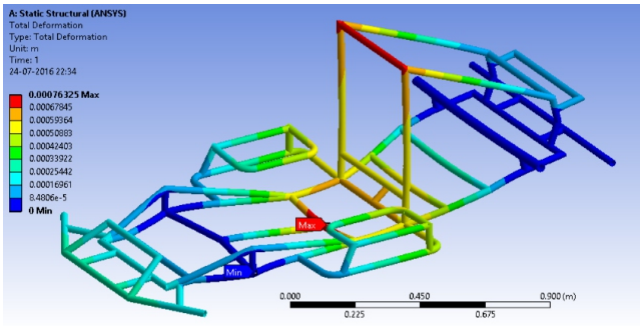

Fig. 11. Deformation Plot in Static Bending Test

As can be seen from the chart, maximum deformation was 0.7 mm at driver seat during sagging which is acceptable. The highest combined stress was encountered at the side bumpers and its value was 129.5 Mpa.

The yield stress of AISI 1020 is 295 MPa. So,

$$FOS = \frac{\text{Max combined stress}}{\text{Yield Stress}} = 2.28$$

So, the minimum FOS evaluated is 2.28 which is safe against an industrial reference value of 1.5. So our design is validated for static bending.

Torsional Stiffness test

This test determines the resistance offered by the chassis frame against a twist which is normally developed during cornering, or when the vehicle encounters a bump in the road.

TABLE 4: LOADING DIAGRAM

Loads	Driver, Engine gravity loads at mounting position A moment of 1000 Nm applied on the axle of chassis
Constraints	Front Wheel Hub mounting position
Gravity	On

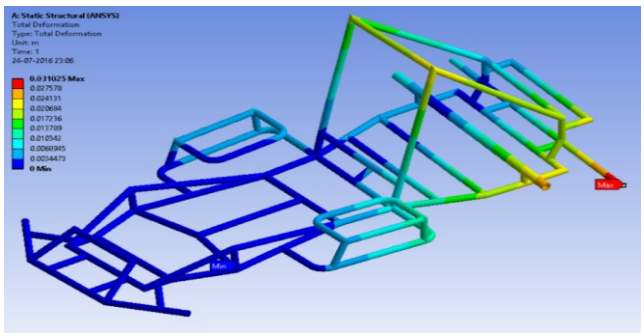

Fig. 13. Deformation Plot in Torsional Stiffness Test

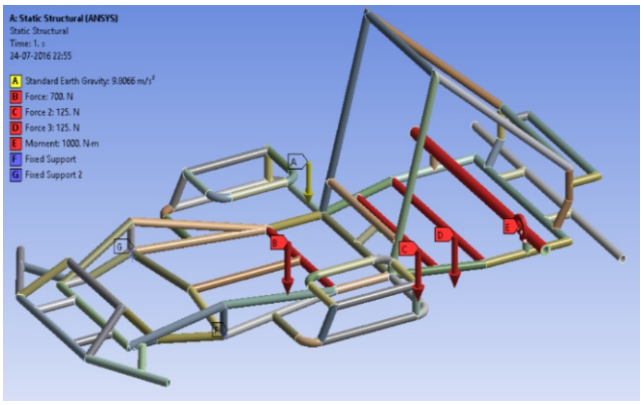

Fig. 12. Loading Diagram of Torsional Stiffness Test

Directional Deformations at the ends of the axle are 10mm and 26mm.

$$\text{Twist} = \tan^{-1}\frac{D_1 + D_2}{L} = \tan^{-1}\frac{36}{850} = 2.422 \text{ degrees}$$

$$\text{Torque} = 1000\text{Nm}$$

$$\text{Torsional Rigidity} = \frac{\text{Torque}}{\text{Twist}} = \frac{1000}{2.422} = \frac{412.88 \text{ Nm}}{\text{deg}}$$

Since this value lies within the standards adopted, it is acceptable.

Front Impact test

This test determines the effect of a crash on the chassis at speeds up to 70 km/h (determined to be the maximum speed when brakes are applied at least for 0.5 seconds before crash).

The collision time in a chassis without a crumple zone is statically averaged to 150ms. But the chassis of this go kart has an mild steel bumper and a thin deformable tube which can act as a crumple zone and increase the collision time to 300ms.

$$F.t\,(\text{Impulse}) = m * \Delta v$$

$$F = m * \left(\frac{\Delta v}{\Delta t}\right) = 160 * \frac{70 - 0}{0.3} * \frac{5}{18}$$

$$F = 10.4 \text{ kN}$$

TABLE 5: LOADING DIAGRAM

Loads	10.4kN applied on front cross members
Constraints	Rear cross members
Gravity	On

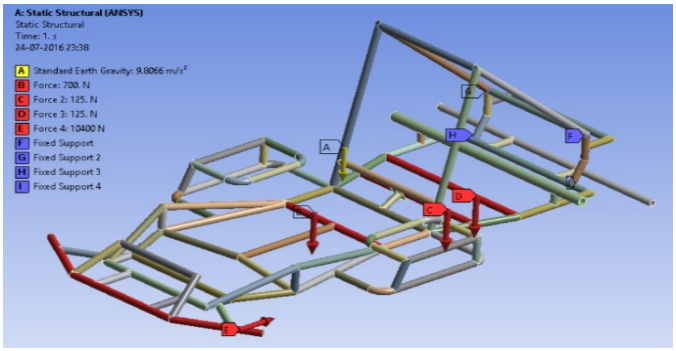

Fig. 14. Loading Diagram of Front Impact Test

The FOS of the front cross members amount to 2.2 which indicates that they will not fail during collision. However the FOS in the cockpit has a minimum value of 5 which is safe enough.

Our model can be said to be validated against front impact test at a speed of up to 70 km/h against an industrial reference value of 1.5.

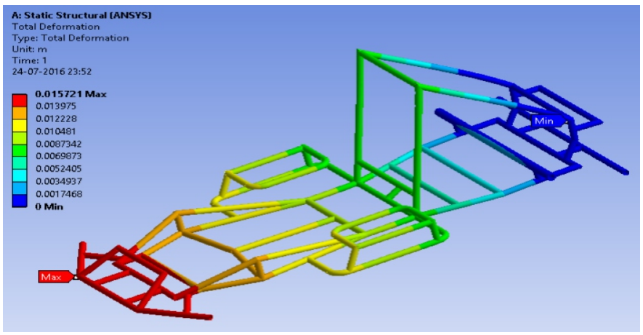

Fig. 15. Maximum Deformation Plot in Front Impact Test

Side Impact Test

This test determines the effect of a crash on the chassis when another kart collides with it on the side members at an angle of 45 degrees. The maximum speed difference between the karts in such a collision is taken to be 25 km / hr. The collision can be modelled as two component forces acting on the side members with a resultant equal to total force applied which are calculated below.

Suppose the test chassis is at rest and another chassis collides into it at a relative speed of 25 km/h at 45 degrees. We apply the momentum theory to this situation considering e=0.5.

$$v_1 - v_2 = 0.5 * 25 * \frac{5}{18} = 3.47 m/s$$

$$\text{and}, v_1 + v_2 = 25 * \frac{5}{18} = 6.94 m/s$$

$$\text{Then } v_1 = \frac{6.94 + 3.47}{2} = 5.22 m/s$$

$$F.t\ (\text{Impulse}) = m * \Delta v$$

$$F = m * \left(\frac{\Delta v}{\Delta t}\right) = 160 * \frac{5.22 - 0}{0.150}$$

$$F = 5.56\ kN \text{ at } 45 \text{ degrees}$$

TABLE 6: LOADING DIAGRAM

Loads	5.56kN applied on side pod members
Constraints	Front and Rear wheel mounts on opposite side
Gravity	On

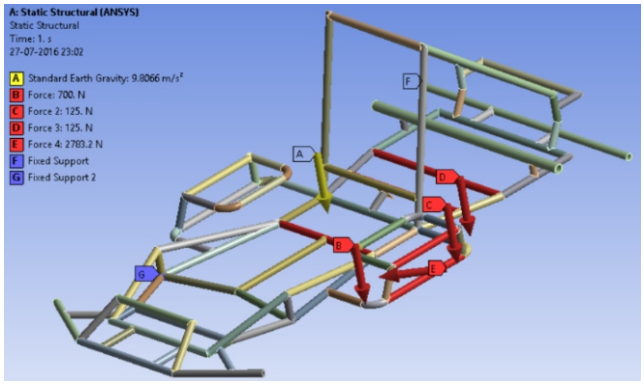

Fig. 16 Loading Diagram in Side Impact Test

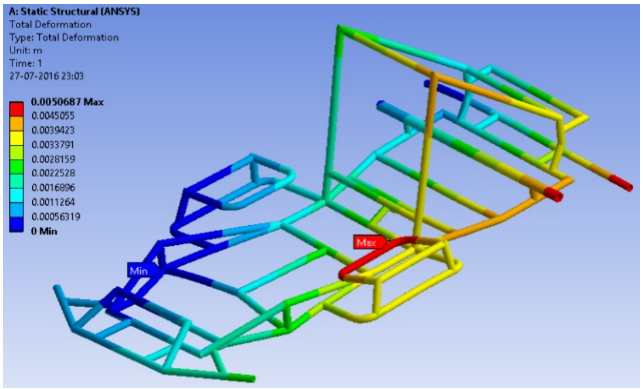

Fig. 17 Maximum Deformation Plot in Side Impact Test

The FOS of the cockpit amounts to 1.3 which indicates that they will not fail during collision. However the FOS in the cockpit has a minimum value of 3 which is safe for the driver. Our model can be said to be validated against side impact test at a speed difference of up to 25 km/h against an industrial reference value of 1.5.

III. ERGONOMICS PURPOSE

Ergonomics is the study of designing equipment and devices that fit the human body and its cognitive abilities. In this project the design of the go kart should be such that all its controls should be comfortably in the reach of the driver's upper body.

Also the vision of the driver should be unobstructed by any part of the go kart as in a dynamic event, vision plays a key role in the driver's and ultimately kart's performance.

METHODOLOGY

Ergonomic analysis for the kart was performed in CATIA v5 R20 using its Human Builder and Human Activity Analysis workspaces. The test model or the manikin was first selected on the basis of the stature of team driver. Details are given in Table 7.

TABLE 7: MANIKIN PROPERTIES

PROPERTY	**VALUE**
Population	Korean
Percentile	50
Height	1702mm
Weight	70kg
Posture	Custom
Cg Height From Ground	525 Mm

The manikin was then positioned into the kart using I-K behaviours and posture-editing.

The Fig. 18 shows the manikin model positioned in the kart which shows that the knees should be bended outwards for maximum comfort. The red dot represents the CG of the driver.

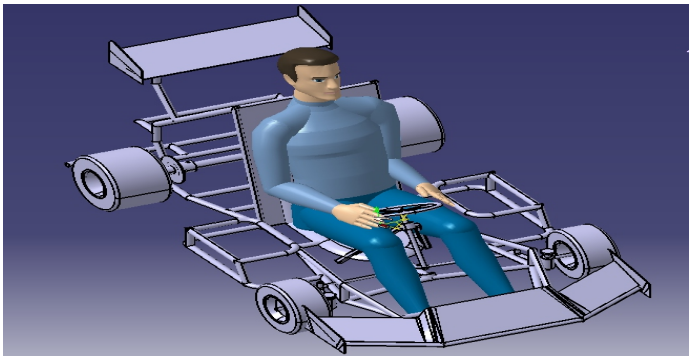

Fig. 18 Ergonomic Model Isometric

The Fig. 19 shows the peripheral vision contours from the driver's point of view in binocular vision mode. The clear area in the middle represents good focus while the blurred region represents unfocussed vision range. In the shown field of vision there is no blurred region. The solid red contour shows the blind spots of the driver without moving.

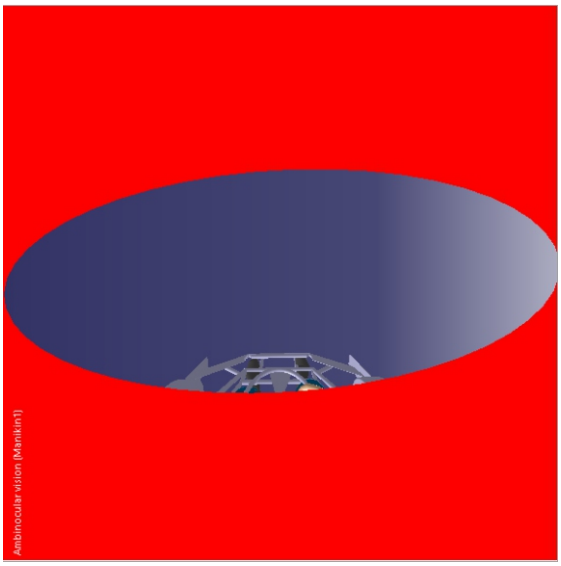

Fig. 19 Field Of Vision

The Fig. 20 shows the upper limb reach that the driver has while bending his upper body and extending his arms. This gives the possible locations of various control switches to be positioned in the kart.

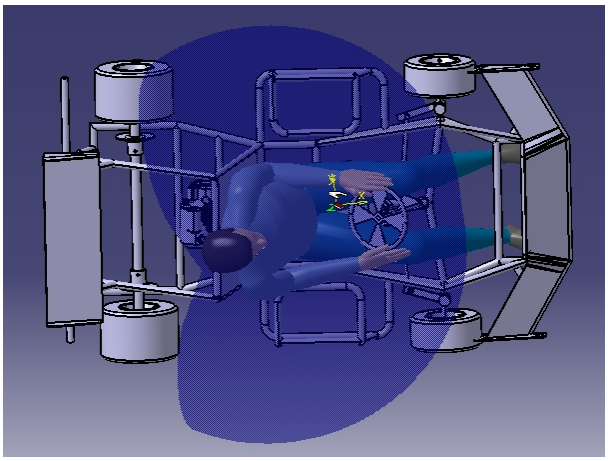

Fig. 20 Reach Envelope

Next an upper limb movement test was performed on the test model to evaluate the reaction performance of the driver in the current posture setting. This test is known as RULA (Rapid Upper Limb Assessment).

The driver model was evaluated by RULA and an average score of 3 was given.

This score category shows that the driver does have a fine reflex action. This score may be attributed to correct posture application in the model.

CONCLUSION

The present paper introduces a new design concepts for the design of go-kart chassis. The various in depth analyses performed on the design iterates and ensures that it meets the industrial safety standards. Focuses has been laid on the new safety features which are feasible to implement and also monumental in an ever changing scientific landscape.

REFERENCES

[1] Singh., A. Jain., P., K. and Gupta. A. "Design analysis of the chassis for the go-kart", ISFT Conference, 18-22 January 2016.

[2] Wakeham., K., J. Introduction to Chassis Design, 1st ed., Memorial University of Newfoundland and Labrador, 2009.

[3] National Kart Racing Championship Rulebook, Season 3, 2016.

[4] Stone., R. and Ball., J., K. Automotive Engineering Fundamentals, 1st ed., SAE International, 2004.

[5] Meriam., J., L. and Kraige., L., G. Engineering Mechanics Statics, 7th ed., Vol. 1, John Wiley & Sons, Inc., 2012.

[6] Meriam., J., L. and Kraige., L., G, Engineering Mechanics Dynamics, 7th ed., vol. 2, John Wiley & Sons, Inc., 2012.

Harmonic Analysis of First Stage Gas Turbine Blade Made of 1N738 Alloy

Sushila Rani[1] Atul K Agrawal[2]

Department of Mechanical, Production, Industrial and Automobile Engineering, Delhi Technological University, Delhi -110042, India

A B S T R A C T

The paper deals with the harmonic analysis of first stage IN738 gas turbine blade by means of experimental modal analysis and finite element method. The frequency response function FRFs of the turbine blade are obtained by an impulse response technique using an impact hammer on the turbine blade and measuring vibration response by an accelerometer. Both the excitation and response signals are fed into the vibration analyzer for computing FRFs. The modal parameters, i.e. frequency, damping and mode shapes are estimated by applying Global Rational Fraction Polynomial method, a global curve fitting of frequency response measurements using the Rational Fraction Polynomial method on a set of FRFs. A finite element model of the first stage IN738 gas turbine blade is created using three dimensional scanning technique and the modal parameters extracted from the finite element analysis are to be compared with the experimental modal analysis results. Numerical (Finite element model) results show excellent agreement with the experimental modal analysis results.

Keywords - Experimental modal analysis, IN738 First Stage Gas Turbine Blade, Mode, Harmonic analysis, Resonant frequency

I. INTRODUCTION

For understanding and solving structural dynamics problems, the experimental modal analysis and finite element modeling are commonly used to extract modal parameters. The experimental modal analysis can be used to obtain the modal model from the measured FRF data. The relationship established between the vibration response at one location and excitation at the same or another location as a function of excitation frequency is known as frequency response function (FRF). Frequency response functions are usually obtained by applying the system input artificially through some type of exciter, i.e. either impact hammer or magnetic shaker; different types of excitation can be imparted including stepped sinusoid, transient, random or white noise [1]. The input is usually measured by a force transducer at the driving point while the response is measured by the accelerometers or other probes. Both the excitation and response signals are fed into an analyzer for computing the FRF data [2]. Numerical (finite element analysis) and experimental modal analysis have become two pillars in modern structural dynamics.

[1]Assistant Professor, Mechanical, Production, Industrial and Automobile Engineering, Delhi Technological University, Delhi-110042, India, sranidtu@gmail.com

[2]Associate Professor, Mechanical, Production, Industrial and Automobile Engineering, Delhi Technological University, Delhi-110042, India, akadce@gmail.com

There are numerous methods in categories of indirect methods and direct methods available to extract the modal parameters from a set of measured FRF's. The indirect methods are based on the modal model, i.e. on the modal parameters (frequency, damping and mode shape) while the direct methods are based on the spatial model (mass, stiffness and damping matrix coefficients). For the analysis of turbine blade, indirect method Global Rational Fraction Polynomial method (GRFP) has been applied for estimating modal parameters, i.e. frequency, damping and mode shapes [3-6].

Tsai et al. [7] performed shaker test for experimental modal analysis on a blade disk. His experimental set up consisted of accelerometer mounted on the blade–disk. He used MEscope software to perform the analysis of measured data to get the mode shapes and natural frequencies. He found that the results obtained from the experimental data agree very well with the results from the finite element analysis. Griffin et al. [8] introduced Fundamental Mistuning Model (FMM) for the prediction of vibratory response of a bladed disk system. Their experimental modal analysis setup consisted of excitation source, laser vibrometer and spectrum analyzer; FMM Software was used for the analysis of measured data in order to compute system properties. Choi et al. [9] worked on the investigation of blade failure in a gas turbine. They performed an impact test of the blade using the fixed boundary condition established using a bench-vice; the natural frequencies and mode shapes for the fixed boundary condition were found experimentally and numerically. The frequencies were calculated using SAMCEF software. On comparison, they observed that natural frequencies showed good agreement except for the second mode; this was because the second mode was generated from the lateral motion of the fixed blade, and the vice could not fully constrain the lateral motion. Rao et al. [10] worked on the failure analysis of compressor blade. In view of the blade failure in stage R3 of the compressor, they carried out Modal testing on a few blades in each of the lower stages using impact hammer and accelerometer. Each blade was impacted at 15 locations and response was picked up by three accelerometers; the real and imaginary functions of Frequency Response Functions (FRFs) showed peaks corresponding to the modal frequencies of the blade.

In this paper a first stage gas turbine blade of 30 MW gas turbine made of nickel based super alloy Inconel 738LC, having operating temperature 1100^0C and has been failed after rendering useful service of 1, 30,000 hrs is harmonically analyzed by means of experimental modal analysis and finite element (FE) method. The experimental analysis is performed using a combination of impulse hammer, accelerometer and Vibration analyzer, which generated a set of frequency response functions. The modal parameters, i.e. natural frequencies, modal damping and mode shapes are extracted by applying Global Rational Fraction Polynomial method (GRFP), on a set of FRFs. A finite element model of first stage IN738 gas turbine blade is developed and harmonic analysis performed using Finite Element Software, ANSYS. The resonant frequencies extracted from the finite element model are compared with the experimental modal analysis results. The numerical (Finite element model) results show excellent agreement with the experimental modal analysis results.

The paper is organized in seven sections. The section two deals with the theoretical background for the estimation of modal parameters by applying GRFP method on a set of FRFs. The section three provides the

details of experimental set-up used for Experimental modal analysis on the First stage IN738 Gas turbine blade. The section four provides results of the estimation of modal parameters from the measured FRF's. The section five provides results of the Finite element Modal Analysis of the First stage IN738 Gas turbine blade. In section six the comparison of both experimental and numerical results is provided. The section seven contains the conclusions.

II Theoretical Background:

Mathematically, the modes of vibration are defined by certain parameters of a linear dynamic model of a structure. The dynamic properties of a structure can be written as a set of differential equations in the time domain, Eq. (1) or as a set of equations containing transfer functions in the Laplace (frequency) domain, Eq. (2)

$$[M]\{\ddot{x}(t)\}+[C]\{\dot{x}(t)\}+[K]\{x(t)\}=\{f(t)\} \quad (1)$$

where [M],[C] and [K] are the mass, damping and stiffness matrices respectively along with the corresponding acceleration $\{\ddot{x}\}$ and the external force {f(t)} applied to the system.

By taking Lapalace transform of Eq.(1) , one may write the equation as or

$$\begin{aligned}&[[M]s^2+[C]s+[K]]\{X(s)\}=\{F(s)\} \quad (2)\\ &[B(s)]\{X(s)\}=\{F(s)\}\end{aligned}$$

The frequency response function is defined as the system transfer function along the frequency axis, and is defined as the inverse of the system matrix

$$[B(s)]^{-1}=[H(s)]=\frac{Adj[B(s)]}{det[B(s)]}=\frac{[A(s)]}{det[B(s)]} \quad (3)$$

In partial fraction form, frequency response function is written as

$$[H(s)]_{s=j\omega}=[H(j\omega)]=\sum_{k=1}^{m}\frac{[A_k]}{(j\omega-p_k)}+\frac{[A_k^*]}{(j\omega-p_k^*)} \quad (4)$$

Thus, transfer function is

$$h_{ij}(j\omega)=\sum_{k=1}^{m}\frac{a_{ijk}}{(j\omega-p_k)}+\frac{a_{ijk}^*}{(j\omega-p_k^*)} \quad (5)$$

Where, $p_k=-\sigma_k+j\omega_d$ = k^{th} pole a_{ijk} = residue for k^{th} pole σ_k = damping co-efficient, ω_d = damped natural frequency and w = undamped natural frequency

For a model with n degrees-of-freedom, it is clear that the FRF contains n pole pairs. Every pole has a different residue associated with it. For six modes, Eq.(5) can be decomposed as

$$\begin{aligned}h_{ij}(j\omega)=&\frac{a_{ij1}}{(j\omega-p_1)}+\frac{a_{ij1}^*}{(j\omega-p_1^*)}+\frac{a_{ij2}}{(j\omega-p_2)}+\frac{a_{ij2}^*}{(j\omega-p_2^*)}+\frac{a_{ij3}}{(j\omega-p_3)}+\frac{a_{ij3}^*}{(j\omega-p_3^*)}+ \quad (6)\\ &\frac{a_{ij4}}{(j\omega-p_4)}+\frac{a_{ij4}^*}{(j\omega-p_4^*)}+\frac{a_{ij5}}{(j\omega-p_5)}+\frac{a_{ij5}^*}{(j\omega-p_5^*)}+\frac{a_{ij6}}{(j\omega-p_6)}+\frac{a_{ij6}^*}{(j\omega-p_6^*)}\end{aligned}$$

Modal properties are evidenced by the resonance peaks which appear in the FRFs measurements. The modal frequency is closely related to the frequency of a resonance peak, and is often approximated by using the peak frequency itself. The modal damping is evidenced by the width of the resonance peak, and can be approximated as one-half of the difference between the two frequencies on either side of the peak where the FRF value is equal to .707 of the peak value. These two frequencies are known as the half- power points. The mode shapes are evidenced by the heights of the resonance peaks, and are commonly obtained by joining the resonance peak values from a set of FRFs measurements [3-6]

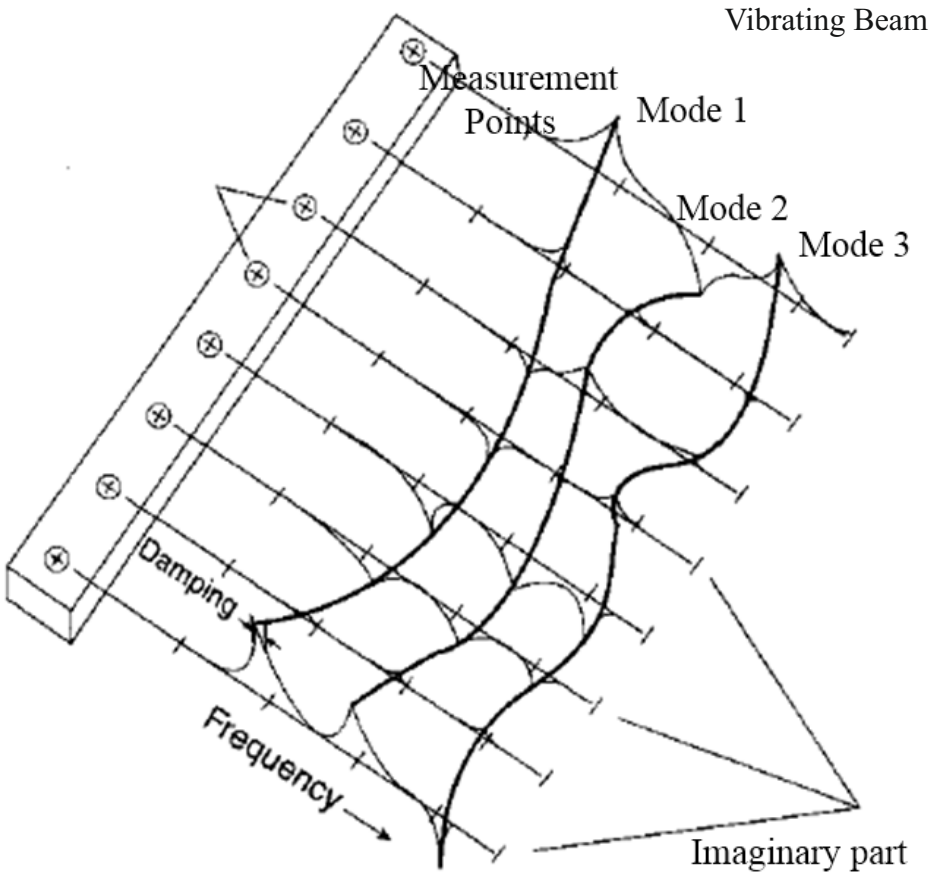

Fig. 1: Global Rational Fraction Polynomial method, (GRFP)

III Experimental Setup

In order to measure the frequency response functions of the turbine blade, one end of the turbine blade is fully constrained in order to prevent all displacements; the boundary conditions are similar to that of cantilever. This boundary condition was established using a fixture.

3.1 Measurement Set Up:

The frequency response function measurement setup is shown in Fig. 2. In addition to the turbine blade, it consists of four main parts: a turbine blade fixture, a PCB-78534 accelerometer, a PCB-086C03 impact hammer and a vibration analyzer OROS. At the start of the experiment, the input range, the frequency range and resolution, triggering, windowing, averaging and hammer tip are selected.

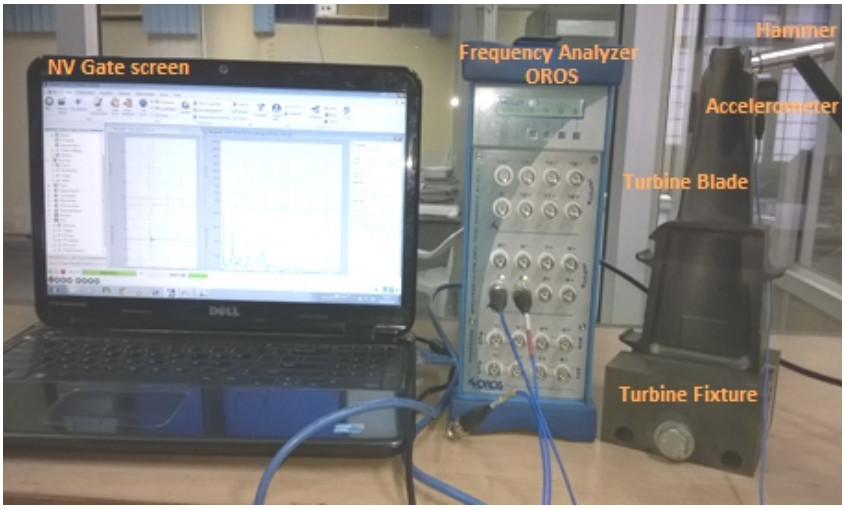

Fig.2: The FRF Measurement Setup

IV Estimation of Modal Parameters

Modal parameters, i.e. natural frequency, damping, and mode shape of the first stage IN738 gas turbine blade are estimated by applying Global Rational Fraction Polynomial method on a set of measured FRFs.

4.1 Modal Frequency:

FRF measured at location 1 while performing experimental modal analysis on the first stage IN738 gas turbine blade is shown in Fig. 3.In this figure, six dominant resonance peaks around approximately 484, 1475, 1810, 2550, 2950 and 3450Hz are identified. Six of these modes are dominant modes as they appear clearly in measured FRFs. Therefore, the first six natural frequencies of turbine blade are 484, 1475, 1810, 2550, 2950 and 3450Hz. The figure also shows a resonance peak around 2160 Hz. This mode is also dominant and clearly appears as an eigenmode. Around 50, 300 and 4100 Hz, possible resonance peaks are present but these are not distinct enough to identity them as resonance peaks. These three modes are almost indistinguishable in the figure but they are nevertheless taken into consideration. The most likely reasons behind the weak appearance of these modes are: the modes are physically less relevant, the modes were insufficiently excited and/or the modes were incompletely measured.

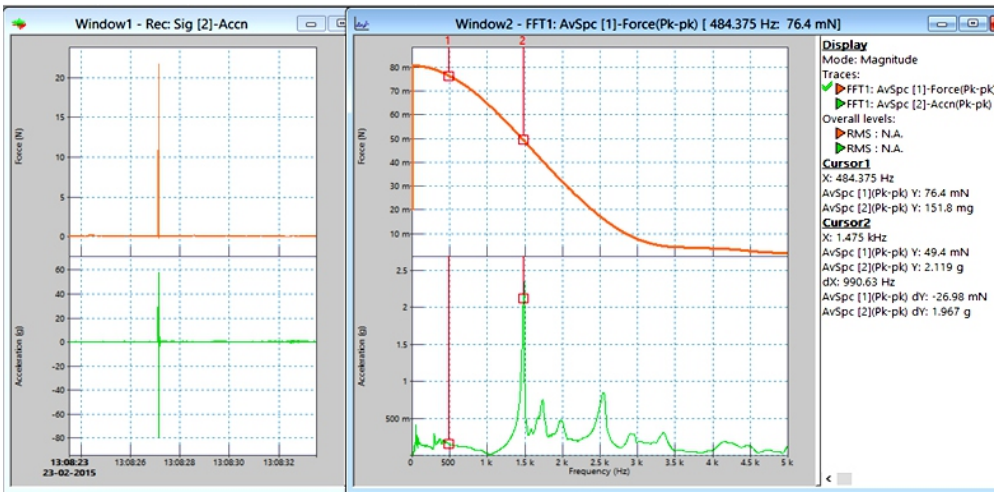

Fig. 3: FRF Measured at Location 1

4.2 Modal Damping:

Modal damping is evidenced by the width of the resonance peak, and calculated using half power method Fig. 4.

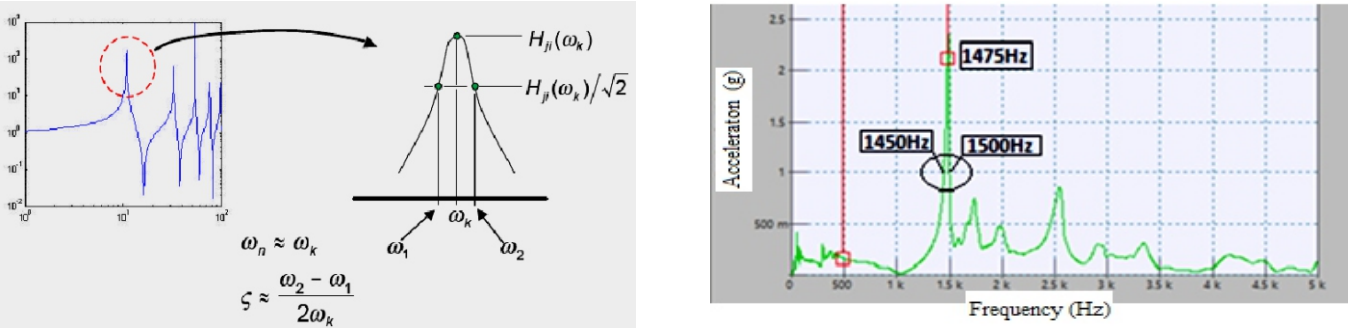

Fig. 4: Modal damping estimation fromthe measured FRF, (GFRP) Method

$$\xi = \frac{\omega_2 - \omega_1}{2 \times \omega_K} \quad (16)$$

$\xi_1 = \frac{494-478}{2\times 484} =$	$\xi_2 = \frac{1500-1450}{2\times 1475}$	$\xi_3 = \frac{1840-1780}{2\times 1810}$
$\xi_4 = \frac{2575-2490}{2\times 2550}$	$\xi_5 = \frac{3000-2900}{2\times 2950}$	$\xi_6 = \frac{3490-3375}{2\times 3450}$

4.3 Mode Shape:

In order to obtain the mode shapes of turbine blade, consider the imaginary part of the amplitude (acceleration/force) versus frequency diagram**,** FRFs Fig. 5. Mode shapes of the first stage IN738 gas turbine blade are obtained by joining the peak values of each of the resonance peaks which occur at the same frequency in all of the FRFs measurements. For example mode 1 of the turbine blade is obtained by joining peak values at natural frequency 484 Hz at all the measured locations starting from the measured location 6 to the measured location 1. Similarly mode shapes 2, 3, 4, 5 and 6 are obtained by joining peak values at natural frequencies 1475, 1810, 2550, 2950 and 3450Hz respectively. All six mode shapes are shown in Fig. 6.

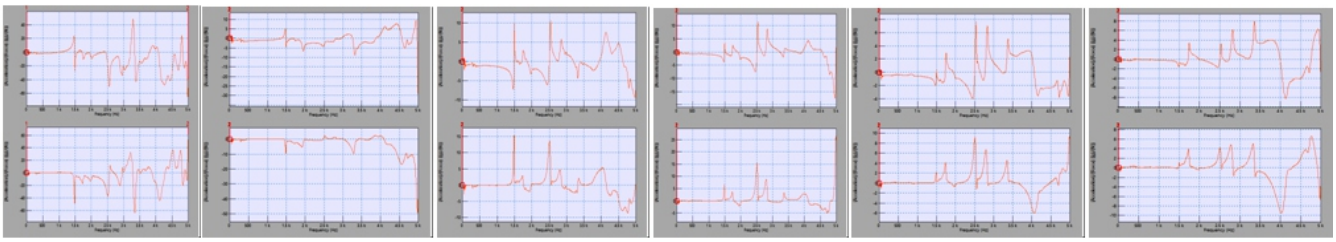

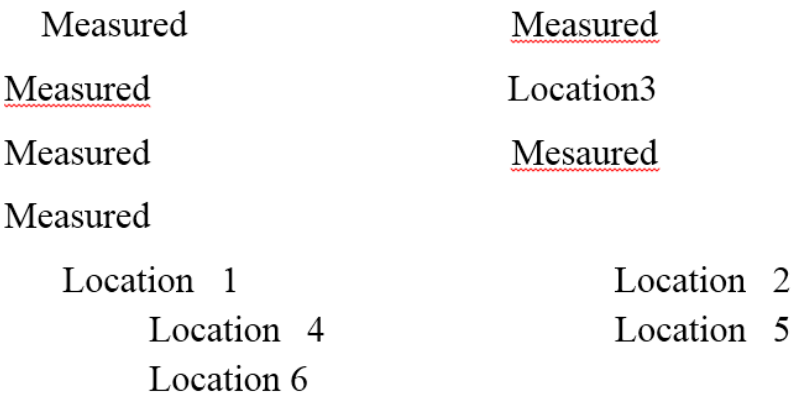

Fig. 5: Real and Imaginary part of amplitude (acceleration/force) versus frequency FRFs

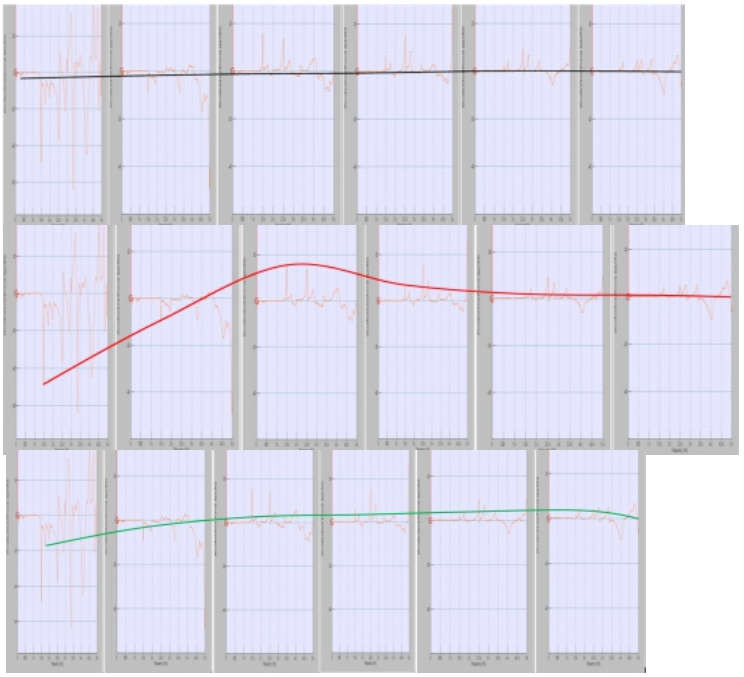

Mode 1 at frequency 484.375Hz

Mode 2 at frequency 1475Hz

Mode 3 at frequency 1810Hz

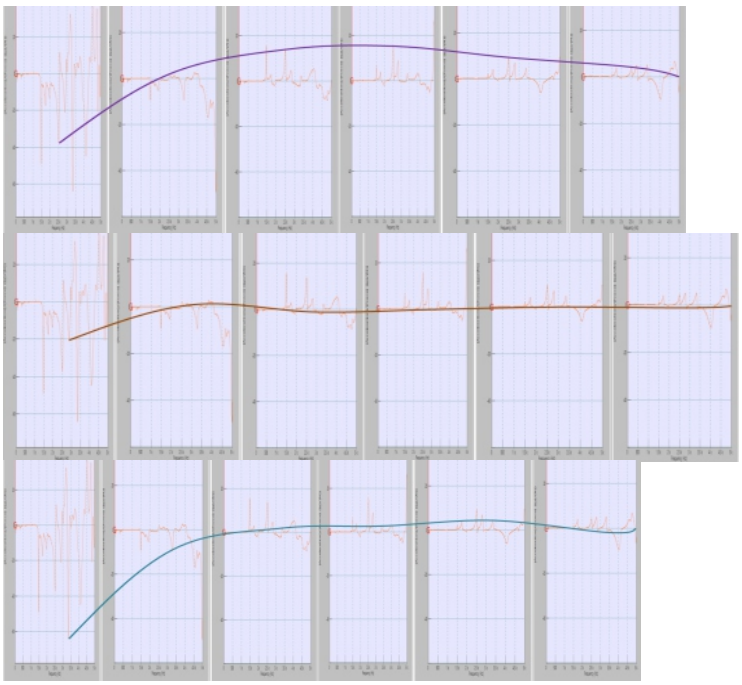

Mode 4 at frequency 2550 Hz

Mode 5 at frequency 2950 Hz

Mode 6 at frequency 3450Hz

Material	Young's Modulus ($N/m^{2)}$	Poisson's Ratio	Density (Kg/m^3)	Bulk Modulus (N/m^2)	Shear Modulus (N/m^2)	Tensile Yield Strength (N/m^2)	Tensile Ultimate Strength (N/m^2)
IN738	$1.3996x10^{11}$	0.3	8110	$1.1664x10^{11}$	$5.3832x10^{10}$	$3.4474x10^{8}$	$4.5505x10^{8}$

Fig. 6: Mode shapes of IN738 first stage gas turbine blad

V Finite Element Modal Analysis Of IN738 First Stage Gas Turbine Blade

The finite element model of IN738 first stage gas turbine blade is developed by using three dimensional scanning technique Fig. 7(a).The modeling and post-processing are performed on finite element based software ANSYS. The finite element model generated has 136468 nodes and 84361 elements Fig. 7(b). Triangular surface mesh is made followed by volumetric meshing using auto meshing features of ANSYS 15. The boundary conditions of the finite element model are similar to that of a cantilever. The turbine blade surface, clamped to the fixture, is constrained by the tie constraints to the fixture surface, and the fixture is, in turn, given fixed boundary conditions on its outer surfaces. The material properties and dimensions of IN738 turbine blade are listed in Table1 and Table 2 respectively. The material properties and dimensions of mild steel turbine blade fixture are listed in Table 3 and Table 4 respectively.

Table 1: Material properties of IN738 Turbine Blade

Table 2: Dimensions of IN738 gas turbine blade (size of bounding box)

Material	Young's Modulus ($N/m^{2)}$	Poisson's Ratio	Density (kg/m^3)	Bulk Modulus (N/m^2)	Shear Modulus, (N/m^2)	Tensile Yield Strength (N/m^2)	Tensile Ultimate Strength (N/m^2)
IN738	$2x10^{11}$	0.3	7850	$1.1667x10^{11}$	$7.6923x10^{10}$	$2.5x10^{8}$	$4.6x10^{8}$

Length, L,(m)	Breadth,b,(m)	Depth, h,(m)
0.25	0.11	0.054

Length, L,(m)	Breadth,b,(m)	Depth, h,(m)
0.11	0.11	0.05

Table 4: Material properties of structural steel turbine fixture

Table 3: Dimensions of structural steel turbine fixture (size of bounding box)

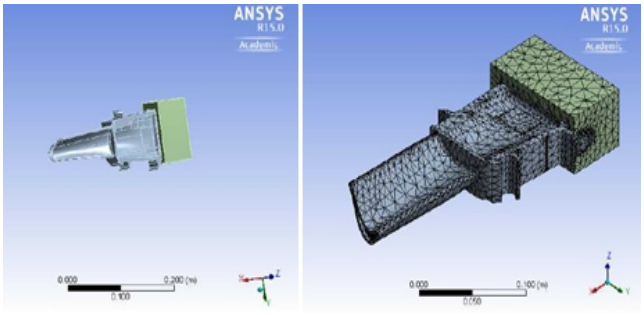

Fig. 7(a): 3-D Model of IN 738 gas turbine blade Fig. 7(b): Mesh model of IN 738 first stage gas turbine blade

The frequency response function of IN738 First Stage Gas Turbine Blade is obtained by performing harmonic analysis on ANSYS as shown in Fig. 8.

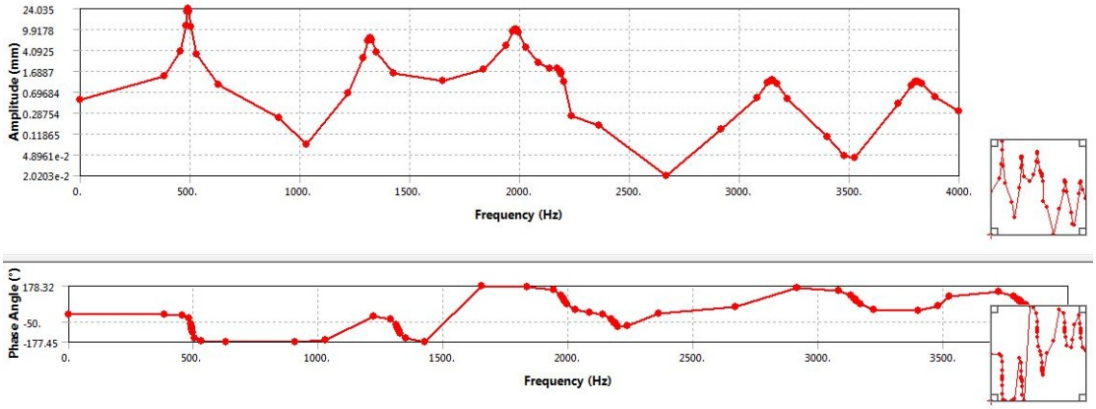

Fig.8: Harmonic Analysis of First Stage Gas Turbine Blade

VI Results and Discussions

The resonant frequencies of IN738 extracted from harmonic analysis using finite element software, ANSYS and the experimental modal analysis are shown in Table 1.

The modal parameters of IN738 first stage gas turbine blade estimated from a set of FRFs by applying GRFP method agree well with the modal parameters extracted from finite element model. The percentage difference calculated between the experimental modal analysis results and the harmonic analysis results is mostly is within 7%. Graphical representation of this comparison is shown in Fig. 9

Table 7: Comparison of resonant frequencies obtained through GRFP method & harmonic analysis

Mode	HMA Results Frequency [Hz]	EMA Results Frequency [Hz]	Error [%] b/w HMA Results & EMA Results
Mode 1	92.16	84.0	1.60
Mode 2	319.5	319.5	0.00
Mode 3	940.40	810.0	6.72
Mode 4	668.88	550.0	4.40
Mode 5	150.43	950.0	6.30
Mode 6	450.5	450.0	0.12

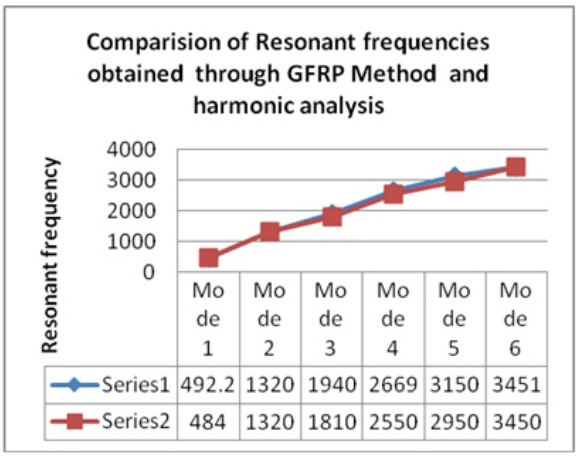

Fig.9: Comparison of resonant frequencies obtained through harmonic analysis and GRFP

VII Conclusions

1.Modal analysis can be a powerful tool for assisting in the identification and elimination of fatigue problems arising in the turbine blade. The first application of modal analysis is in the determination of dynamic characteristics of turbine blade and the second application of modal analysis is in the validation of computer generated models of the turbine blades. These models can be very useful for investigating the turbine and turbine blade properties under running conditions.

2. The modal parameters of the first stage IN738 gas turbine blade, i.e. natural frequency, damping, and mode shape are estimated from a set of FRFs by applying Global Rational Fraction Polynomial (GRFP) method.

3. The modal parameters of IN738 first stage gas turbine blade estimated from a set of FRFs agree well with the modal parameters extracted from the finite element analysis. The percentage difference between the experimental modal analysis results and the finite modal analysis results is within 7 %.

VIII References

[1] Jimin, He. and Zhi-Fang, Fu. , "Modal Analysis" ISBN 0 7506 5079 6, Butterworth-Heinemann publications 2001.

[2] Maia, N. M. M., Silva, J. M. M., "Theoretical and Experimental Modal Analysis", Ed.: Maia & Silva, Publ. Research Studies Press, Distrib. John Wiley & Sons, 1997.

[3]Fillod, R., Lallement, G., Piranda, J., Raynaud, J. L., "Global method of modal identification", proceedings of the 3'd International Modal Analysis Conference (IMAC lll), vol. II, Orlando, Florida, U. S. A., pp-1145-1151, 1985.

[4] Richardson, M. H. & Formenti, D.L., "Parameter Estimation from Frequency Response Measurements using Rational Fraction Polynomials", Proceedings of the 1st International Modal Analysis Conference, Orlando, Florida, November 8-10, 1982.

[5] Richardson, M. H. & Formenti, D. L. "Global Curve Fitting of Frequency Response Measurements using the Rational Fraction Polynomial Method", Proceedings of the 3rd International Modal Analysis Conference, Orlando, Florida, pp 390-397, January 28-31, 1985.

[6] Formenti, D. and Richardson, M. H. "Global Frequency & Damping from Frequency Response Measurements", Proceedings of the 4th International Modal Analysis Conference, Los Angeles, California, February 3-6, 1986.

[7] Gwo-chung Tsai, "Rotating vibration behavior of the turbine blades with different groups of blades", Journal of sound and vibration, Vol. 271, pp- 547-575, 2004.

[8]Griffin J. H., Feiner D.M.,"Fundamental Mistuning Model for determining system properties and predicting vibratory response of bladed disks", Patent No.-US7082, 371B2, July 25, 2006.

[9] Choi Yeon-Sun," Investigation of blade failure in a gas turbine", Journal of Mechanical Science and Technology, Vol. 24, No.-10, pp- 1969-1974, June 2010.

[10] Rao. A. R., Dutta B. K.,"Vibration analysis for detecting failure of compressor blade" Journal of Engineering Failure Analysis, Vol. 25, pp- 211-218,2012.

Heat Transferin Microchannel Heat Sink: Review

Sunny Chandra[1]‡, Om Prakash[2]
1Mechanical Engineering Department, Research Scholar, N.I.T Patna
sunnychandra27@gmail.com,
2Mechanical Engineering Department, Professor, N.I.T Patna
om.prakash@nitp.ac.in
‡ Corresponding Author: 8987260099

A B S T R A C T

High performance computers, avionics, defense systems require powerful cooling systems like micro-channel heat sink to dissipate large amount of heat flux. The microchannel heat sink is usually made from high thermal conductivity materials with the high surface area to have high heat transfer with lower temperature differences. Micro-channelsfabricatedto have high surface area by micro-machining technology. The heat sink features flow boiling of working fluid through a series of parallel micro-channels with cross-sectional dimensions ranging from 10 to 100 μm. The objective of this paper is collectively present the work done by different researchers on the heat transfer mechanism in microchannel heat sink in laminar flow conditions. Two phase heat transfer in microchannel heat sink is more effective than single phase heat transfer as two phase heat sinks dissipates high heat fluxes at smaller flow rate of working fluid in comparison to single phase heat sinks at same temperature difference. Effect of variation of two phase heat transfer coefficient with Reynolds number (Re) and aspect ratio (β) is presented in this paper. Two phase heat transfer coefficient shows increasing trend with Reynolds number and aspect ratio.

Keywords - Microchannel heat sink; Heat transfer mechanism in microchannel heat sink; two phase heat transfer coefficient.

ABBREVIATIONS

W	:	Width of copper block (cm)
L	:	Length of copper block (cm)
W_{ch}	:	Width of micro-channels (ì m)
H_{ch}	:	Height of micro-channels (ì m)
W_w	:	Width of wall separating the micro-channels (ì m)
D_h	:	Hydraulic diameter (ì m)
T_w	:	Maximum wall temperature at the channel outlet (?)
h_t	:	Two phase heat transfer coefficient (W/m^2K)
A_{ch}	:	Area of microchannel (m^2)
Nu_3	:	Nusselt number for laminar fully-developed flow for three wall heat transfer
Nu_4	:	Nusselt number for laminar fully-developed flow for four wall heat transfer
â	:	Aspect ratio

1. INTRODUCTION

Due to the faster signal speed and superior performance of electronic devices, the past two decades have witnessed exceptional increases in heat dissipation in high performance computers, electrical vehicle power electronics, avionics, and directed energy laser and microwave weapon systems. Today localized heat dissipation from advanced microprocessors has already exceeded 100 W/cm2, while high-end defence application such as lasers, microwave devices and radars are beginning to exceed 1000 W/cm2, whereas in nuclear reactors needs heat flux removal rate of 10000 W/cm2 [1]. Requirement for heat dissipation will continue to rise with the improvement in technologies and further reduction in the size of these applications.

Heat fluxes for different applications are shown in figure 1. Trends of cooling technologies adopted to meet the steep increase in heat fluxes over the years are shown in figure 2. The exponential curve shows the increase in the heat flux and changes in the cooling technologies. Powerful cooling systems are needed to face the challenges of emerging technologies as well as to make possible further developments in these technologies that will

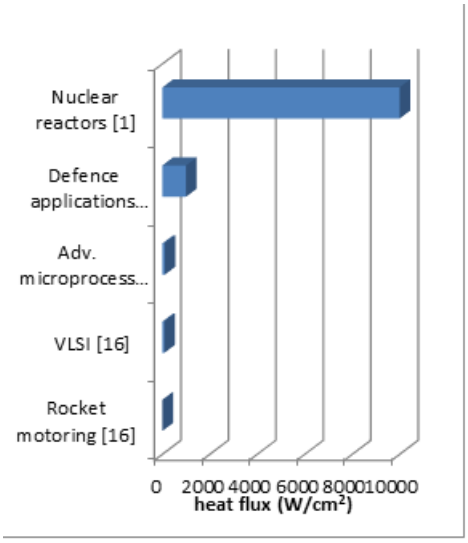

Figure 1: Variation of dissipation of heat fluxfor different applications

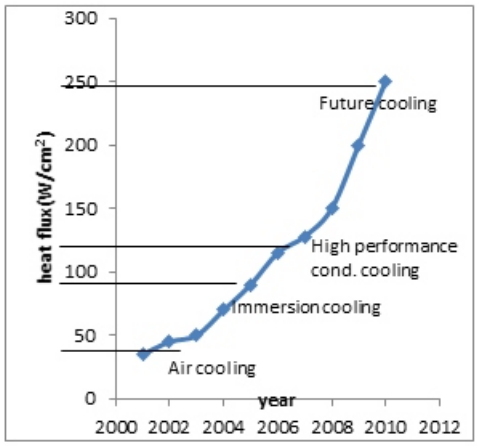

Figure 2: Variation of cooling of Heat flux with required due to developmentof new technology in different fields [16].

increase the heat dissipation. Various cooling systems have been developed to achieve the desired. These consist of pool boiling thermosyphons, channel flow boiling, jet and sprays etc [2]. The concept of micro-channel heat sink was first introduced by Tuckerman and Pease in the early 1980s. Micro-channel heat sink is an inventive cooling technology which removes large heat fluxes from a small volume. The heat sink is usually made from high thermal conductivity materials such as silicon or copper with the micro-channels made-up into its surface by either precision machining or micro-fabrication technology. Micro-channels have characteristics dimensions ranging from 10 to 1000 μm [3] and they serve as flow passages for the working fluid. Very high surface area to volume ratio, large convective heat transfer coefficient, small mass and volume, and small coolant inventory make heat sink very suitable for cooling devices like microprocessors, laser diode arrays, radars, and high-energy-laser mirrors [4]. Micro-channel heat sinks can be categorised as single phase and two phase. The coolant may maintain its liquid single phase state throughout micro-channels for a fixed dissipative heat flux and high flow rate which corresponds to a single-phase heat sink. If coolant flow rate is comparatively low, the liquid coolant may reach its boiling point while flowing in micro-channels and flow boiling occurs, which results in a two-phase heat sink. Two phase heat sinks are ideally suited for dissipating large amount of heat within very limited space which is demand of the modern applications. These devices are light weight and compact, and needs very small coolant inventory.

The objective of this paper is to understand the heat transfer phenomena in microchannel heat sink by presenting a review on the different parameters which affects two phase heat transfer coefficient in microchannel heat sink under laminar flow condition.

2. HEAT TRANSFER IN MICRO-CHANNEL HEAT SINK

Heat transfer mechanism in micro-channel heat sink is different for subcooled and saturated boiling conditions because of the void fractions. In subcooled boiling liquid flow is abundant phase change happens mostly by bubble formation at the wall, while saturated flow boiling in microchannels is governed by two mechanisms: nucleate boiling and forced convection boiling [3]. In the nucleate boiling dominant region, liquid near the heated channel wall is superheated to an adequate degree to maintain the nucleation and growth of vapour bubbles. The heat transfer coefficient in this region is dependent upon heat flux, but less susceptible to mass velocity and vapour quality. The nucleate boiling region is normally related with the bubbly and slug flow patterns, and the forced convection boiling region related to the annular flow pattern. Qu & Mudawar [5] measured the incipient boiling heat flux in a heat sink containing 21 rectangular micro-channels 231 μm wide and 713 μm. Tests were performed with deionized water as coolant at inlet velocities of 0.133-1.44 m/s, inlet temperatures of 30, 60 & 90oC at an outlet pressure of 1.2 bar. Their findings were that at incipient boiling, a small number of nucleation sites appear at the same time close to the exit of several micro-channels, with one or two sites per micro-channel. In the forced convection boiling dominant region, large heat transfer coefficient causes suppression of bubble nucleation along the heated wall, so the heat is transferred mainly by single-phase convection through the thin annular liquid film and carried away by evaporation at the liquid–vapor interface. Qu & Mudawar [3] tested the heat transfer characteristics at a mass velocity range of 135-402 kg/m2s, inlet temperatures of 300C, 600C, and at outlet pressure of 1.17 bar. Results indicated an unexpected transition to annular flow near the point of zero thermodynamic equilibrium quality, and exposed that dominant heat transfer mechanism is forced convective boiling corresponding to annular flow. The heat transfer coefficient in this region depends on coolant mass velocity and vapour quality, but independent of heat flux. Saisorn et al. [6] has studied experimentally the heat transfer characteristics of air–water flow in horizontal micro-channels. The tests were performed at a heat load of 80 W, with superficial Reynolds numbers of gas and liquid ranging between 54–142 and 131–373, respectively. Two inlet sections with different designs were used in this work to investigate the dependency of Nusselt number on flow characteristics. The experiments exposed that the development of small gas slugs instead of gas core flow involves an increase in Nusselt numbers due to which gas–liquid flow gave heat transfer enhancement up to 80% over the liquid flow. Mirmanto [7] performed experiments to investigate local heat transfer coefficients during flow boiling of water in a rectangular microchannel. The hydraulic diameter of the channel was 0.635 mm. The nominal mass fluxes varied from 200 to 700 kg/m2s and heat fluxes in the range of 171 to 685 kW/m2 were applied. An inlet fluid temperature of 98 °C and pressure of 125 kPa were maintained at the microchannel entrance. Results showed that heat transfer is dominated by nucleate boiling and the effect of quality suppresses the local heat transfer coefficient.

2.1 Effect of working fluid other than water on heat transfer performance of microchannel heat sink

In most of studies water is used as working fluid but water is not an appropriate working fluid for removing large amounts of heat from electronic devices because of its current carrying capacity and corrosive nature [8]. Now

some researchers have moved to Freon based refrigerants like FC-72, FC-77 because of its high dielectric constant due to which these refrigerants can withstand at very high heat fluxes. But Freon's have also some limitations because of its ozone layer depletion rate which is harmful for environment. Hence now a day's some eco-friendly refrigerants like R134a, R123, R410a, HFE-7000, HFE-7100 etc. are employed as coolant in the test module to solve the problems of corrosiveness and ozone layer depletion. Nascimento et al. [9] performed an experimental investigation of a micro-channel heat sink based on flow boiling of R134 in micro-channels. The results showed that the heat-sink average heat transfer coefficient increases with increasing mass velocity for a fixed mean vapour quality. Dong et al. [10] investigated flow boiling of Freon R141b in rectangular microchannel heat sinks. Experiments were performed over mass velocities ranging from 400 to 980 kg/m2s and heat flux from 40 to 700 kW/m2, and atmospheric pressure at outlet. The results showed that the mean heat transfer coefficient of R141b flow boiling in present microchannel heat sinks depends greatly on mass velocity and heat flux. Lee & Mudawar [11] explored the cooling performance of microchannel heat sink using HFE7100 for four different microchannel sizes. Results revealed that heat fluxes in excess of 700 W/cm2 could be managed without burnout.

2.2 Effect of channel and heat sink geometry on heat transfer in micro-channel heat sink

Channel and heat sink geometry plays important role in heat transfer performance analysis of a micro-channel heat sink. Liu et al. [12] studied the heat transfer performance of the high pin fins with the Reynolds number ranging from 60 to 800 using deionized water as working fluid. The studies were carried out for micro square pin fins of 559 X 559 μm2 and 445 X 445 μm2 cross-section. They has concluded that heat dissipation rat Xe could reach 2.83 X 106 W/m2 at the flow rate of 57.225 L/h and the surface temperature of 73.40C for 445 X 445 μm2, also heat resistance decreased with increase in pressure drop. Prajapati et al. 2015 [13] compared the flow boiling characteristics of deionized water in three different configurations of micro-channels through experimental investigations. The investigated channel configurations were uniform cross-section, diverging cross-section and segmented finned micro-channels. Experiments have been conducted with subcooled liquid state at the entry and varying coolant mass and heat fluxes. For entire operating conditions, segmented finned channels demonstrate the highest heat transfer coefficient. Peles et al. 2005 [14] investigated experimentally the heat transfer phenomena over a bank of micro pin fins. It has been observed that very low thermal resistances are achievable using a pin fin heat sink as compared tomicro-channel convective flows, therefore heat transfer performance has been improved for the devices using micro pin fins. Deng et al. [15] has compared the flow boiling performance of reentrant microchannels (REEM) and conventional rectangular microchannels (RECM) at the same hydraulic diameter. Comprehensive comparative experiments with two coolants, i.e., deionized water and ethanol, were performed at inlet sub-cooling of 100C and 400C, and mass fluxes of 200–300 kg/m2s. Experimental results showed that the re-entrantmicrochannels present significant rise in two-phase heat transfer in large inlet subcooling cases and moderate to high heat fluxes.

Two phase heat transfer coefficient investigations for different authors has been compared at different Reynolds

number (Re) and different aspect ratio (β). In figure 3. two phase heat transfer coefficient result at Re= 200-600 for different investigations has been plotted. Two phase heat transfer coefficient shows increasing trend with Reynolds number from figure 5. It can be understand that higher aspect ratio is beneficial for dissipating high heat fluxes as increase in Nusselt number ratio of three wall and four wall heat transfer leads to enhancement in two phase heat transfer coefficient.

Table 1: Summary of heat transfer investigations

Author	Dimensions of MCHS	Input Parameters	Contribution
Qu &Mudawar.[4]	W= 1.0 cm, L= 4.48 cm, Rectangular channels N= 21,W_{ch}= 231 W_w= 118 H_{ch}=713	Coolant- Deionized water, Re= 139-1672 q'= 100W/cm^2 and 200 W/cm^2Investigation- single phase flow	heat transfer characteristics of micro-channel heat sinks can be effectively predicted using Navier-Stokes and energy equations
Qu &Mudawar. [3]	-same-	-same-	The saturated flow boiling heat transfer coefficient is a strong function of mass velocity, and only a weak function of heat flux and thermodynamic equilibrium quality.
Qu &Mudawar [2]	Rectangular channels N=21, W_{ch}= 215µm, W_w= 125µm H_{ch}= 821µm	T_{in}= 30 & 60^0 P_{out}= 1.13 bar, G= 86-368 kg/m^2s	The results show that as CHF was approached, flow instabilities induced vapour backflow into the heat sink's upstream plenum
Nascimento et al. [9]	Copper (28 mm X 25 mm), Rectangular parallel W_{ch}= 100µm, W_w= 200 µm, H_{ch}= 500µm, N=50	Coolant- R134a G=400-1500 kg/m^2s, q'= upto 310 kW/m^2,saturation temperature at outlet = 25℃	heat-sink averaged heat transfer coefficient increases with increasing mass velocity for a fixed mean vapour quality.
Saisorn et al. [6]	Rectangular channels W_{ch}=450µm,W_w= 540µm, H_{ch}= 410µm, N= 21,L_{ch}= 40 mm	Q= 80W, Re for gas= 54-142, Re for liquid= 131-373	The gas–liquid flow gave heat transfer enhancement up to 80% over the liquid flow
Liu et al. [12]	Copper substrate (20 mm X 20 mm Micro square pin fins of 559 X 559 µm^2 and 445 X 445 µm^2 cross-section.	Coolant-deionized water Re =60-800	heat dissipation rate could reach 2.83 X 10^6 W/m^2 at the flow rate of 57.225 L/h and the surface temperature of 73.4^{0}C for 445 X 445 µm^2.

Author	Dimensions of MCHS	Input Parameters	Contribution
Dong et al. [10]	W= 0.5 cm, L = 2 cm Rectangular channels W_{ch}=60 µm, W_w= 60 µm, H_{ch}= 200 µm,N= 50	Coolant- R141b G= 400 to 980 kg/m^{2}s and q'= 40 to 700 kW/m^2	mean heat transfer coefficient of depends greatly on mass velocity and heat flux.
Mirmanto[7]	copper channel (12 mm × 25 mm × 72 mm.) W_{ch}=1710 µm ,H_{ch}= 390 µm, W_w=1190 µm	Coolant-water, G= 200 to 700 kg/m^{2}s q'= 171 to 685 kW/m^2 T_{in}= 98 °C & p_{in}= 125 kPa	heat transfer is dominated by nucleate boiling and the effect of quality suppresses the local heat transfer coefficient.
Prajapati et al. [13]	Copper(25.7 mm X 12.02 mm) Rectangular	Coolant- deionized water, G= 100-350 kg/m^{2}s, T_{in}= 30°C, Re= 50-500 q'=10-350kW/m^2	highest heat transfer coefficient was observed for segmented finned channels as compared to other two configurations of channels for entire operating conditions.
Lee &Mudawar [11]	Rectangular channels W_{ch}=123.4 µm, 123.4µm, 235.2 µm, 259.9 µm, W_w= 84.6 µm, 84.6 µm, 230.3 µm, 205.0 µm, H_{ch}= 304.9 µm, 526.9 µm, 576.8 µm, 1041.3 µm, N= 24, 24, 11, 11	Coolant- HFE-7100, T_{in}= -30°C, 0°C, P_{out}= 1.138 bar, m= 2.0- 5.0 g/s	Heat transfer performance of the micro-channel heat sink can be greatly enhanced by lowering the temperature of coolant entering the heat sink.
Deng et al. [15]	copper block (20 mm x 45 mm)Reentrant porous (convex Ω shaped) channels N=14, D_h=786 µm Cavity size=10- 50 µm	Coolant-deionized water & ethanol, T_{in} subcooled= 10^{0}C & 40^{0}C, G= 200–300 kg/m^{2}s, Re= 200-700	two-phase heat transfer showed Signiant rise in large inlet sub cooling cases and moderate to high heat fluxes for the reentrant channels as compared to con-ventional rectangular channels.
Peles et al. [14]	Silicon substrate, cylindrical pin fins of (1.8 mm wide and 243 µm deep with length 10 mm)	De ionized water Re=200-800 q'=790 W/cm^2.	Very high heat fluxes can be dissipated at low wall temperature rise using a microscale pin fin heat sink.

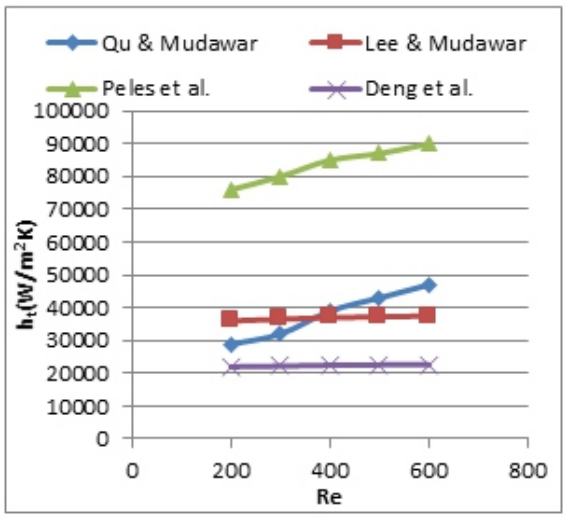

Figure 3: Reynolds number (Re) Vs Two phase heat transfer coefficient (h_t).

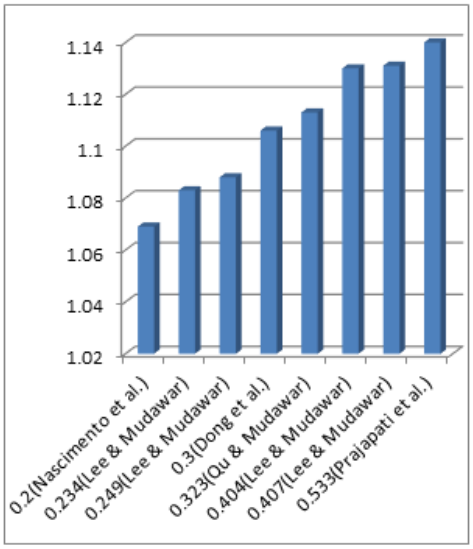

Figure 4: Aspect ratio (β) Vs Nusselt number ratio of three wall and four wall heat transfer (Nu_3/Nu_4)

RESULT AND CONCLUSIONS

Heat transfer mechanism in microchannels is different for saturated and subcooled flow boiling conditions. Saturated flow boiling conditions are governed by nucleate and forced convection. The nucleate boiling region is associated with the bubbly and slug flow patterns while forced convection boiling is related to the annular flow. In subcooled flow phase change occurs mostly by bubble formation at the wall.

Two phase heat transfer coefficient enhances with augmentation in Reynolds number (Re) due to which performance of microchannel heat sink will be improved in laminar flow conditions.

Two phase heat transfer coefficient enhances with increase in Nusselt number ratio of three wall and four wall heat transfer due to enhancement in aspect ratio.

From the above review work one can concludes that heat transfer coefficient is having close relation with the Reynolds number but different coefficient of increments. The coefficient of increment is a factor of operating conditions.

REFERENCES

[1] J. Lee, I. Mudawar, Fluid flow and heat transfer characteristics of low temperature two-phase micro-channel heat sinks- Part 1: Experimental methods and flow visualization results, International Journal of Heat and Mass Transfer, vol.51, pp 4315–4326, 2008.

[2] W. Qu & I. Mudawar, Measurement and correlation of critical heat flux in two-phase micro-channel heat sinks, International Journal of Heat and Mass Transfer, vol. 47, pp 2045–2059, 2004.

[3] W. Qu & I. Mudawar, Flow boiling heat transfer in two-phase micro-channel heat sinks-I, Experimental investigation and assessment of correlation methods, International Journal of Heat and Mass Transfer, vol. 46, pp 2755–2771, 2003

[4] W. Qu, I. Mudawar, Experimental and numerical study of pressure drop and heat transfer in a single-phase micro-channel heat sink, International Journal of Heat and Mass Transfer, vol. 45, pp 2549–2565, 2002.

[5] W. Qu, I. Mudawar, Prediction and measurement of incipient boiling heat flux in micro-channel heat sinks, International Journal of Heat and Mass Transfer, vol. 45, pp 3933–3945, 2002.

[6] S. Saisorn, P. Kuaseng, S. Wongwises, Heat transfer characteristics of gas–liquid flow in horizontal rectangular micro-channels, Experimental Thermal and Fluid, vol. 55, pp 54–61, 2014.

[7] M. Mirmanto, Local pressure measurements and heat transfer coefficients of flow boiling in a rectangular microchannel,Heat Mass Transfer, vol.52, pp 73-83, 2016.

[8] S.T. Kadam, R. Kumar, Twenty first century cooling solution: Microchannel heat sinks-A Review, International Journal of Thermal Sciences, vol. 85, pp 73-92, 2014.

[9] F.J.D Nascimento, H.L.S. Leao, G. Ribatski, An experimental study on flow boiling heat transfer of R134a in a microchannel-based heat sink, Experimental Thermal and Fluid Science, vol. 45, pp 117–127, 2013.

[10] T. Dong, Z. Yan, Q. Bi, Y. Zhang, Freon R141b flow boiling in silicon microchannel heat sinks: experimental investigation, Heat Mass Transfer, vol. 44, pp 315–324, 2008.

[11] J. Lee, I. Mudawar, Fluid flow and heat transfer characteristics of low temperature two-phase micro-channel heat sinks- Part 2. Subcooled boiling pressure drop and heat transfer, International Journal of Heat and Mass Transfer, vol. 51,pp 4327–4341, 2008.

[12] M. Liu, D. Liu, S. Xu, Y. Chen, Experimental study on liquid flow and heat transfer in micro square pin fin heat sink, International Journal of Heat and Mass Transfer, vol. 54, pp 5602–5611, 2011.

[13] Y. K. Prajapati, M. Pathak, M. K Khan, A comparative study of flow boiling heat transfer in three different configurations of microchannels, International Journal of Heat and Mass Transfer, vol. 85, pp 711-722, 2015.

[14] Y. Peles, A. Kosar, C. Mishra, C.J Kuo, B. Schneider, Forced convective heat transfer across a pin fin micro heat sink, International Journal of Heat and Mass Transfer, vol.48, pp 3615-3627, 2005.

[15] D. Deng, W. Wan, H. Shao, Y. Tang, J. Feng, J. Zeng, Effects of operation parameters on flow boiling characteristics of heat sink cooling systems with reentrant porous microchannels, Energy Conversion and Management, vol. 96, pp 340-351, 2015 340–351.

[16] Thermal Management in Electronic Equipment, HCL Technologies, February 2010

Key Technologies of using Hydrogen as a IC Engine Fuel in Indian Scenario

‡*Gurpreet Singh and *Amit Pal

*Department of Mechanical Engineering, Delhi Technological University, Main Bawana Road, Delhi, India

(guru.singh1111@gmail.com, amitpal@dce.ac.in)

‡ Corresponding Author; Gurpreet Singh, Tel: +91 8802774224,

E Mail : guru.singh1111@gmail.com

ABSTRACT

Hydrogen fuels are most promising and clean fuel in future most effective environment friendly fuel, and its benefits are remarkable for cleaning the environment. This article is based on hydrogen benefits and technique of storage, sustainability in future scope. Increasing the price of conventional fuel, rate of increasing the Green House Gasses and energy security concerns so moving towards to the alternative fuels. Key Technologies of using Hydrogen as a IC Engine Fuel in Indian perspective are discussed in this paper.

Keywords - Hydrogen; Fuel Cell; Gasification; Hythane

1. INTRODUCTION

As using the conventional fuels since the eighteen century, the fuels are about to end and the level of emission is tremendously increased. We have started move towards to direction of non conventional fuels, hydrogen comes for more promising fuel which is more efficient, reliable also odourless, colourless fuel. Hydrogen has been introduced to engine as a fuel since 1920s(1) . The energy content in terms of mass 120.7 MJ/kg. Particularly GHGs is coming from automobile and commercial industries which play the major role for increasing emission,petroleum fuels, hydrogen is clean (pollution free), renewable and environmentally friendly. When it burns, it releases only water vapour into the environment. There are no spilling or pooling concerns because it dissipates quickly into the atmosphere [2] Hydrogen is an ideal fuel and versatile energy carrier, and its advantages are summarized as below [3]:.

(a) Easy to produce.

(b) Convenient fuel for transportation.

(c)Versatile, converts easily to other energy forms at the user end.

(d) High utilization efficiency.

(e) Environmentally compatible (zero- or low-emission).

The Hydrogen energy is the only renewable energy which can provide clean commercial energies, the

electricity and the fuel for transport which is to obtained from the chloral alkali industries, petroleum refineries & fertilizer plants,Production of hydrogen is still limited [4]. Hydrogen from coal gasification may be equally undesirable because of its high emissions when carbon sequestration is not used, Hydrogen from nuclear power has much lower emissions than electrolysis, Gasification has been shown to exhibit an economy of scale and is a suitable conversion technology for large demand centers [5].

However, several barriers have to be overcome before hydrogen electric vehicles can be put into large-scale practical utilization. One of the most severe challenges is the lack of a safe and efficient onboard storage technology, which may dramatically influence the vehicle's cost, range, performance, and fuel economy, as well as shape the scale, investment requirements, energy use, and potential emis- sions of a hydrogen-refueling infrastructure. That is to say, the development of onboard storage technology will directly determine the schedule of hydrogen-powered vehicles into the market [6].

2. MATERİALAND METHODS

2.1. Industrial benefits

2.1.1. Efficient way by using internal combustion engine (ICE

Hydrogen fuelled have two ways of running in vehicle .One that have an internal combustion engine with a hydrogen fuel tank. Other is that runs on hydrogen fuel cells .With the concern of the foreseen reduction in fossil fuel resources and stringent environmental constraints, the demand of improving internal combustion (IC) engine efficiency and emissions has become more and more pressing. Hydrogen has been proved to be a promising renewable energy that can be used on IC engines[7] . for an S.I. engine can be classified into four categories such as Carburetion, Inlet Manifold Injection, Inlet Port Injection and Direct Cylinder Injection. These conventional methods of 'FIT' could also be applied to engine operation with a non-conventional alternative fuel, such as hydrogen.[8] Due to the high autoignition temperature of hydrogen (approximately 858 K)[7].Hydrogen possesses many unique combustion properties that benefit the engine efficiency and emissions performance. The diffusion coefficient of hydrogen (0.61 cm2/s) is about four times as large as that of gasoline (0.16 cm2/s), which improves the mixing process of fuel and air, and also helps in improving the homogeneity of the combustible mixture. The adiabatic flame speed of hydrogen (237 cm/s) is five times as large as that of gasoline (42 cm/s) which may contribute to improving the engine operating stability. Meanwhile, the high adiabatic flame speed of hydrogen indicates that the combustion of hydrogen engines is much closer to ideal constant volume combustion, which is beneficial for higher thermal efficiency [9]. The combustion of hydrogen with air however can also produce oxides of nitrogen NO_x & it's the only pollutant of concern from the hydrogen engine has been restricted under 100_{ppm} by lean operation strategy[10].

Hydrogen applications, besides industrial application, cover power generation, transport applications and heat. However, when compared to other alternatives, use of hydrogen in transport sector appears to be more beneficial

as it is possible to store hydrogen on-board.

In view of its unique properties, large-scale use of hydrogen in transport sector can help India in achieving energy security through reduction in import of fossil fuels and also reduction in the urban air pollution. Therefore, it is necessary to develop hydrogen energy technologies for large-scale use especially for the transport sector[11]. In contrast, hydrogen tends to dissociate on metal surfaces, diffusing into the metal as a single atom. As hydrogen diffuses into the metal, it interacts with the microstructure affecting properties such as ductility, fracture resistance, and fatigue crack growth; these interactions are generically referred to as hydrogen embrittlement[12]. Hydrogen in materials can evolve from many sources, including corrosion, electrochemical environments and ambient moisture, as well as direct exposure to environments containing gaseous or liquid hydrogen, such as storage and distribution of hydrogen fuels [13].

2.1.2 Hydrogen Fuel Cell

Hybrid renewable energy concept in taking new energy source for participating in reduction the emission .Using the Photovoltaic fuel cell hybrid system ,an alkaline Electrolyser produces hydrogen which is stored in a LaNi5 type Metal Hydride. The hydrogen stored is utilized by fuel cell to generate DC power. Fuel Cell inverter then converts DC power into AC power.

This hydrogen power generation system is integrated with the PV system to form the hybrid PV-FC system[14]. Its clean , high Efficiency, silent and vibration free and reliable benefits makes the good source of fuel.

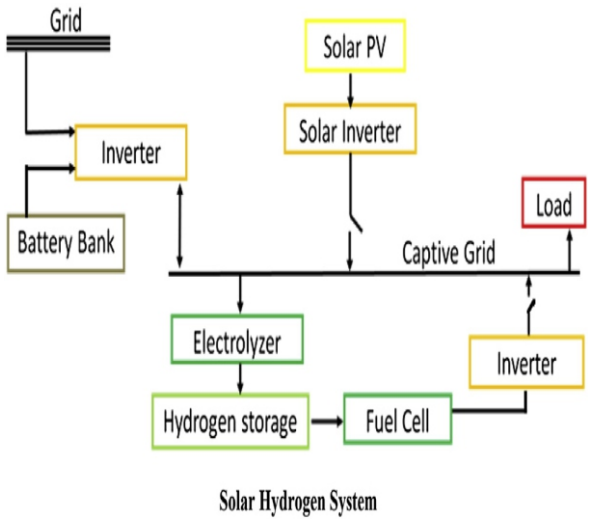

Fig.1: Hydrogen Generation System

2.1.3 Hythane

In this context, introduced simulated the Hydrogen and methane ,Gaseous biofuels have superior energy balances, offer greater greenhouse gas emission reductions and produce lower pollutant emissions than liquid biofuels[15]. In 2008 india adopts Hythane as natural gas regulations planned for augest 2009[16]. This is low cost technology which is proven over twenty-five year, cheapest way to meet new emission standard.

3. Biohydrogen Production using Gasification

India has the highest number of biomass gasification units of any nation – nearly all of these are used for electricity production in rural areas. Other common feedstocks used in Indian gasification units include rice straw, rice husk, cotton stalk, and mustard husk[17]. One benefit of gasification is it offers higher daily production capacity than other biomass to hydrogen pathways like anaerobic digestion, biophotolysis, and fermentation and therefore could potentially be used to meet large-scale energy demand [18]. The *National* Academy of Science declared that hydrogen from biomass gasification "could play a significant role in meeting the DOE's goal of greenhouse gas mitigation" [19].

Table1:Hydrogen vs. other conventional fuels

Fuel property	Hydrogen	Natural Gas	Petrol	LPG
Lower heating value (MJ/kg)	120.7	49.54	41.87-44.19	46.05
Higher heating value (MJ/kg)	141.89	54.89	43.73-47.45	50.24
Density at standard conditions (kg/m3)	0.08	0.6	720-780	510
Phase at standard conditions	Gas	Gas	Liquid	Liquid
Auto-ignition temperature in air (°C)	566-582	540	257	454-510
Ignition limit in air (Vol.%)	4.1-74	5.3-15	1.4-7.6	2.2-9.5
Diffusion coefficient in air (cm^2/s)	0.61	0.16	0.05	0.11

3. 1 Methanol

Use of methanol is one of the common methods of hydrogen production which is done with the help of reformer, where it yields CO,CO2 and H2 gas[20]. As per current statistics, 48% of current hydrogen production comes from natural gas, 30% from oil, 18% from coal and 4% from electrolytic[21]. The genera- tion of hydrogen from diverse domestic resources can reduce the demand for oil by more than 11 million barrels per day by the year 2040, which will require us to convert current gasoline stations to hydrogen stations. The department of energy (DOE) has suggested that the gravimetric density should reach 9 wt% and the volumetric capacity should be 81g of H_2/L [22].

3.2 Benefits With Hydrogen Storage Techniques

Storage is a key issue for the hydrogen economy. It cuts across the production, distribution, safety and applications aspects [23-24]. Hydrogen energy is very efficient fuel source than traditional sources of energy and produces more energy per pound of fuel.

This clearly means that a car loaded with hydrogen fuel with go much farther than the one using same amount of traditional source of energy. In fact, hydrogen is three times as powerful as gasoline and similar fossil fuels, meaning it takes less of it to accomplish more. Storage of hydrogen in chemical compounds offers a much wider range of possibilities to meet the transportation requirements, but no single material investigated to date exhibits all the necessary properties.

One gram of hydrogen gas occupiesw11 L (2.9 gallons) of space at STP, so storage implies a need to reduce the enormous volume occupied by hydrogen. All the practical storage options have disadvantages, but still, the most promising appears to be hydrides. A viable means of hydrogen storage excludes inefficient and risky high-pressure cylinders, expensive cryogenic cylinders and all covalent hydrocarbon compounds[4]. The technical targets for on board hydrogen based light duty vehicles are given in These vehicles should possess an ability to store5–6 kg of hydrogen which will be required to cover an area of around300–350 mile.

Table 2. Department of Energy's technical targets for on board hydrogen systems .Adapted from Ref [26-27].

Storage parameter	2005	2010	2015
Usable specific energy from H2 (kg H2/kg)	0.045	0.06	0.09
Usable energy density from H2 (kg H2/L)	200	133	67
Storage system cost ($kg/H2)	3	1.5	67
Fuel cost ($/gallon gasoline equivalent at pump	- 20/100	- 30/100	- 40/100
Minimum and maximum delivery temp. of H2 from the tank(1C)	-	-	-
Refuelingrate(kgH2/min)	0.5	1.5	2
Loss of usable hydrogen (g/h)kgH2 stored	1	0.1	0.05

Currently hydrogen can be stored in three forms gaseous, liquid or as a solid combined with a metal hydride.

3.2.1 Intermetallic Hydrides

Hydrides hold promise for safe mode of hydrogen storage[4]. and release it later, either at ambient temperature or through heating of the tank. Intermetallic hydrides possess hydrogen storing capacity of 5–7 wt% [25]. The addition of transition metal such as Ti to sodium alanate (NaAlH4), in which Ti stays on the surface and substitutes for Na ion ,tends to attract a large number of H atoms to its vicinity[28]. Mg2NiH4 attracts wide interest for being a promising hydrogen storing material due to its relatively high capacity, lowcost, light weight and low-toxicity and for its unusual structural and bonding properties[29,30].

3.2.2 Carbon Nanomaterials

Porous carbon structure is another interesting system for hydrogen adsorption [31]. Hydrogen gets adsorbed on the surface of carbon through Van der Waals bonding (_6 kJmol_1).Nanotubes. Carbon Nano tubes (CNTs) are micro scopic tubes of carbon [32]. Many improvements have been achieved in synthesizing microporous carbonaceous materials with very high hydrogen adsorption properties [33-34]. CNTs and bucky balls have been modified by transition metals or alkali metals in order to increase the binding of H2 molecules on to metal-CNT hybrids [35]. Since H_2 molecules at elevated pressures on a solid surface are expected to form a close-packed configuration [36]. Addition of nano structured graphite to the LiBH4 system can effectively improve the dehydrogenation kinetics and cyclic stability [37].

CONCLUSION

Dependency of the fossil fuel on the industrial sector is decreasing with increasing of renewable energy. Hydrogen must be the primary fuel in future for reducing the emission level and will able to live in clean atmosphere, few things of beneficial resulted concluded that the their use in automobile industry and storage techniques participating good role globally.

REFERENCE

1) Norbeck JM, Heffel JW, Durbin TD, Tabbara B, Bowden JM, Montano MC. Hydrogen fuel for surface transportation. Warrendale, PA: SAE Inc.; 1996.

2) Zuttel A, Borgschulte A, Schlapbach L. Hydrogen as a future energy. Weinheim: Carrier Wiley-VCH Verlag GmbH & Co. KGaA,; 2008.

3) Veziroglu TN, Barbir F. Hydrogen: The wonder fuel. Int J Hydrogen Energy;vol. 17,pp.391–401, 1992.

4) M. Sterlin Leo Hudson, P.K. Dubey, D. Pukazhselvan, Pandey S. K , Singh R.K , Raghubanshi H, Rohit. R. Shahi, Srivastava O.N. Hydrogen energy in changing environmental scenario: Indian context, international journal of hydrogen energy vol.34, pp.7358 – 7367, 2009.

5) National Academies of Science (NAS). The Hydrogen Economy - Opportunities, Costs, Barrriers, and R&D Needs, National Research Council and National Academy of Engineering, Editor. National Academies Press: Washington, DC, pp. 256,2004.

6) Cheng H.M, Yang Q.H , Chang Liu. Hydrogen storage in carbon nanotubes , Carbon vol. 39 pp. 1447–1454, 2001.

7) Szwaja S, Karol G.R. Hydrogen combustion in a compression ignition diesel engine, international journal of hydrogen energy,Vol. 34 , pp. 4413– 4421 ,2009.

8) Das L.M. Fuel induction techniques for a hydrogen operated engine Int. J. Hydrogen Energy, Vol. 15, No. 11, pp. 833-842, 1990.

9)) Das LM. Hydrogen–oxygen reaction mechanism and its implication to hydrogen engine combustion. International Journal of Hydrogen Energy Vol. 21,pp.703–15,1996

10) Changwei Ji, Shuofeng Wang. Effect of hydrogen addition on combustion and emissions performance of a spark ignition gasoline engine at lean conditions, international journal of hydrogen energy, Vol.34, 7823 – 78 34,2009.

11) National hydrogen energy road map mnre. 2006, http://mnre.gov.in/file-manager/UserFiles/abridged-nherm.pdf

12) San Marchi C, Somerday. BP. Technical reference for hydrogen compatibility of materials. SAND 2012 e7321. Sandia National Laboratories, 2012.

13) C. San Marchi a, E.S. Hecht a, I.W. Ekoto a, K.M. Groth b, C. LaFleur b, B.P. Somerday a, R. Mukundan c, T. Rockward c, J. Keller d, C.W. James. Overview of the DOE hydrogen safety, codes and standards program, part 3: Advances in research and development to enhance the scientific basis for hydrogen regulations, codes and standards, i n t e r n a t i o n a l journal of hydrogen energy 1e12, 2016.

14) L.M. Das, Dutta V. Hydrogen energy activities in India , i n t e rna t i onal journal o f hydrogen energy ,Vol.40: 4280e4283, 2015.

15) Ao Xia a,b, Jun Cheng c, Jerry D. Murphy. A Innovation in biological production and upgrading of and hydrogen for use as gaseous transport biofuel, Biotechnology Advances Vol. 34,pp. 451–472, 2016.

16) Das L.M. Hydrogen vehicle and fuelling infrastrutre in India.2009, http://energy.gov/sites/prod/files/2014/03/f10/cng_h2_workshop_11_das.pdf

17) Hydrogen Energy Board Ministry of New and Renewable Energy Government of India, http://mnre.gov.in/file-manager/UserFiles/abridged-nherm.pdf

18) Morrison G, Kumar R, Chugh S, Puri S.K,Tuli D. K, Malhotra R. K.. The institue of transporation studies, file:///C:/Users/gurpreet/Downloads/2011-UCD-ITS-RR-11-09%20(1).pdf

19) Singh J, Gu S. Biomass conversion to energy in India – A critique. Renewable and Sus-tainable Energy Reviews ,Vol.14 ,pp.1367-1378,2010.

20) Energy Information Administration (EIA). The impact of increased use of hydrogen on petroleum consumption and carbon dioxide emissions. SR-OIAF-CNEAF/2008-04,2008, http://www.eia.doe.gov/oiaf/servicerpt/hydro/hydrogen.html.

21) Yang J, Sudik A ,Wolverton C ,Siegel DJ .High capacity hydrogen storage materials: attributes for automotive applications and techniques for materials discovery. Chem SocRev2010 Vol.39, pp.656–75.

22)Wang L, Yan R T. News or bents for hydrogen storage by hydrogen spill over—a review. Energy Environ Sci 2008,Vol. pp.268–79.

23) Berry G D, McAceves S M. The case for hydrogen in a carbon constrained world. J Energy Resour Technol Vol.127, pp.89–94,2005.

24)Schlapbach L, Zuttel A. Hydrogen-storage materials for mobile applications. Nature, Vol. 414, pp. 353–8, 2001.

25) Schulz R, Huot RJ, Liang G, Boily S, Van Neste A. Structure and hydrogen sorption properties of ball milled Mg dihydride, MaterSci Forum, pp. 312– 314 :615–22,1999.

26) Niaz S, Manzoor T, Pandith A.H. Hydrogen storage: Materials, methods and perspectives, Renewable and Sustainable Energy Reviews, Vol. 50, pp.457-469, 2015.

27) Bouza A, Read C. J, Satyapal S, Milliken J .Annual DOE hydrogen program review ,hydrogen storage, office of hydrogen, fuel cells, and infrastructure technologies , 2004.

28) Iniguez J, Yildirim T. Structure and hydrogen dynamics of pure and Ti-doped sodium alanate. Phys Rev B. Vol.70:060101,2004.

29) Orimo S, Fujii H. Materials science of Mg–Ni-based new hydrides. ApplPhys A. Vol.72 pp.167–86, 2001.

30) SatoT, Blomqvist H, Noreus D.Attempts to improve Mg2Ni hydrogen storage by aluminium addition. JAlloys Compds 2003;356–357:494–6.

31) Zubizarreta L, Arenillas A, Pis JJ. Carbon materials for H2 storage. Int J Hydrogen Energy.Vol. 34,pp. 4575–81,2009.

32) Darkrim F L , Malbrunot P ,Tartaglia G P .Review of hydrogen storage by adsorption in carbon nanotubes.Int J Hydrogen Energy.Vol. 27 pp.193–202, 2002.

33) Froudakis G E. Hydrogen interaction with carbon nanotubes: a review of ab initio studies. J Phys: Condens Matter. Vol. 14: pp.453–65,2002.

34) Gupta B K, Tiwari R S, Srivastava O N. Studies on synthesis and hydrogenation behaviour of graphitic nano fibres prepared through palladium catalyst assisted thermal cracking of acetylene. J Alloy Comp .381:301–8, 2004.

35) Chen P ,Wu X ,Lin J ,Tan K L. High H2 uptake by alkali-dopedcarbonnanotubes under ambient pressure and moderate temperatures Science Vol. 285 pp. 91–3,1999.

36) Dresselhaus M S, Williams K A, Eklund P C. Hydrogen adsorption in carbon Materials. MRS Bull. Vol. 24,pp. 45–50,1999.

37) Wang K , Kang X, Ren J, Wang P ,Nano structured graphite-induced destabilization of LiBH4 for reversible hydrogen storage, Journal of Alloys and Compounds pp.685:242e247,2016.

Low-Cost Manufacturing and Implementation of an Optimized Model of Horizontal Axis Hydrokinetic Turbine and Test Bed Assembly

Suyash Nigam‡[1], Tanmay Nema[2], Vansh Sharma[3], Shubham Bansal[4] and Raj Kumar Singh[5]

[1]Department of Mechanical Engineering, Delhi Technological University, India

suyashnigam@dtu.ac.in, tanmaynema@dtu.ac.in, sharmavansh99gmail.com, shubhambansalrmr@hotmail.com, rajkumarsingh@dce.ac.in,

Tel: +91 7838912711

ABSTRACT

Hydrokinetic turbine is a developing technology which harnesses zero-head free flow of water. This presents a low emission way to satisfy the increasing energy demand of the world, at the same time minimally affecting the hydrological ecology. The primary classification of these turbines is done on the basis of axis of rotation relative to the flow- horizontal (HAHkT) and vertical hydrokinetic turbines with horizontal axis improving on some of the problems of vertical axis ones.

This paper illustrates our methodology to manufacture 3-D printed blade and hub assembly in an economic manner to test the horizontal axis HAHkT in a test bed facility.

Keywords - HAHkT; hydrofoil; chord length; 3-D printing;

1. INTRODUCTION

India, with its emphasis on 'Skill India' and 'Make in India' campaigns is power hungry but deficient today. However, it is blessed with abundance of hydro-electric potential and ranks 5th in terms of exploitable hydro-potential on global scenario. [1-2] States rich in harness able natural water reserves are Maharashtra, Madhya Pradesh, Punjab, Karnataka and Himanchal Pradhesh [3] These turbines have already been tested commercially in several quarters of the world.[4-12]

In this regards, hydrokinetic turbines offer a viable, clean and efficient alternative. These energy conversion systems have a propeller with two or more blades rotating around a horizontal or vertical shaft by the effects of the hydrodynamic forces present in a free stream. Each blade may consist of a single or multiple hydrofoil geometry depending upon the radial distance. The blades rotate with the torque that is produced by the lift or drag force, depending on the orientation.

Each blade section has an optimum angle of attack, which is the angle between the relative velocity and the blade section's chord line. On the other hand, hydrokinetic turbines are subjected to high thrust and torsional loads due to density of water causing high bending moment at the blade root. So, thicker blade sections are preferred near the hub.

Applying the above principles, s832 and e817 profiles were chosen in our work previously along with optimal chord angles and converging results. [13] However the real challenge faced in a project is more often than not in the implementation phase when faced with a myriad of problems. To test the model, a hydrokinetic turbine and associated components were developed.

2. TEST APPARATUS

The primary challenge faced in manufacturing any component is the selection of the material. In our case the material selected for the components of the apparatus is aluminium solely on the fact it is lighter than the available alternative of Mild Steel. Aluminium is a very desirable metal because it is more malleable and elastic than steel. Aluminium can create shapes that steel cannot, often forming deeper or more intricate spinnings. Especially for parts with deep and straight walls, aluminium is the material of choice. Steel is a very tough and resilient metal but cannot generally be pushed to the same extreme dimensional limits as aluminum without cracking or ripping during the spinning process. A look on the table of properties can alleviate further doubts.

Table 1. Comparison of structural properties of steel and aluminium

Properties		Aluminiu	Steel
Density,	Kg m^{-3}	2,700	7,800
Young's Modulus, *E*	N mm^{-2}	70,000	210,000
Shear Modulus, *G*	N mm^{-2}	27,000	81,000
Posisson Ratio, *v*		0.33	0.3
Coefficient of linear thermal expansion, α	K^{-1}	$23 * 10^{-6}$	$12 * 10^{-6}$

Clearly, the density of steel is 2.5 times that of aluminium. Hence the strength to weight ratio of aluminium is higher. Also, considering the serviceability of the apparatus, steel is more prone to rusting whereas aluminium is not. Using mild steel would have required extra strength to the mounts making it heavier and a costly setup. Hence aluminium was preferred naturally.

2.1. Parts Designed

- Hub

Design criterion: The hub mounts the blades and the nose along with a shaft in the center. The square bore was selected to discard the need of a key to prevent relative motion. The 3 holes on the side are given to mount the nose with the help of fasteners.
Material used: Aluminium Manufacturing process undertaken: CNC Wire-Cutting.

The choices available for the manufacturing were CNC-Milling and CNC-Wire Cutting. The process was selected on the basis of the square shape of the bore and lesser time required to manufacture the part. Better dimensional accuracy is achieved with lesser cost.

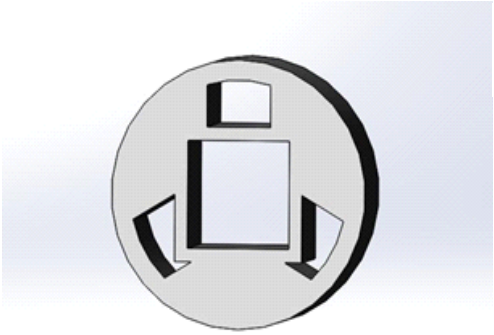

Shaft

Design criteria: The Shaft was made square on the front part to eliminate the need of cutting a keyway and using a key. A bore with M6 tapped dimension is given to mount the pulley at one end.

Material used:Aluminium Manufacturing process undertaken: Lathe work.

Figure 1. Model of Hub

Lathe work was selected, as the part was simple in design and the piece could be quickly manufactured and the cost was null. The part did not require much accuracy as in case of the hub.

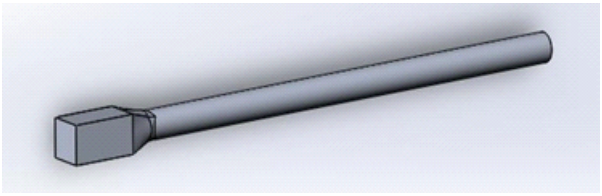

Figure 2. Model of Shaft

Figure 3. Shaft in manufacturing

Blades

Design criteria: The basic profile of the blade model was made up to the height of 12cm. The base mount part was split into two parts to provide a method to test the profile for various angles of attack. The holes provided restrict motion of both parts and the cylindrical extrusion ensures better locking. Material used: ABS (Plastic) Manufacturing process undertaken: 3D printing (with 100% infill).

The blades required high accuracy which is very difficult to achieve as such small scale model by other processes like CNC milling. Also, the cost of 3D printing is less compared to other processes.

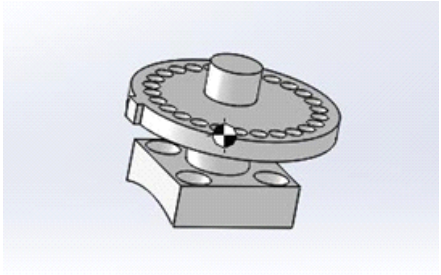

Figure 4. Model of pitch varying mechanism

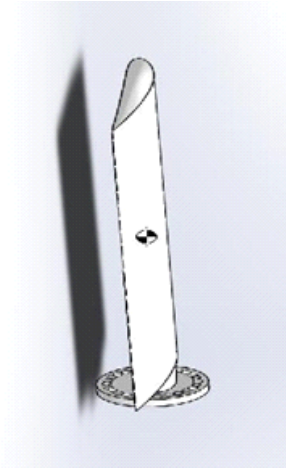

Figure 5. Model of optimised blade

Figure 6. Blade and pitch angle assembly manufacturing

Nose

Design criteria: The nose is designed to minimize drag and for easy mounting to the hub via 3 fasteners.

Material used: ABS (Plastic)

Manufacturing process undertaken: 3D printing (with 100% infill)

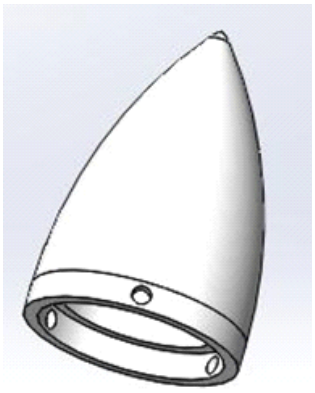

Figure 7. Model of nose

Figure 8. Manufactured of nose

Pulley

Design criteria: The pulleys are designed according to the belt available in the market and the reduction ratio required for the motor. A v-style groove was selected with 1.5mm wall on sides and 3mm depth. The belt thickness was kept 4mm. Material used: ABS (Plastic) and Aluminium.

Manufacturing process undertaken: Lathe work

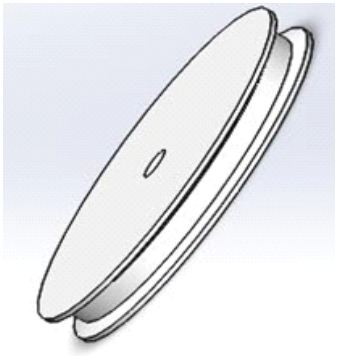

Figure 9. Model of Pulley

Bearing Mounts

Design criteria: The mounts are designed according to the bearing and keeping focus on easy and simple usage. 2 tapped holes are used to fasten the mount to the base plate.

Materialused: Aluminium Manufactruring process undertaken: Lathe work.

Lathe was selected over choices like milling and pantograph due to less wastage of material in manufacturing. Also, the process was cheaper and time saving.

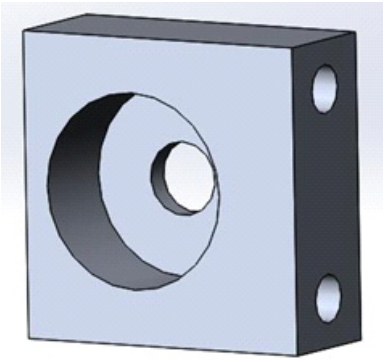

Figure 10. Model of bearing mounts

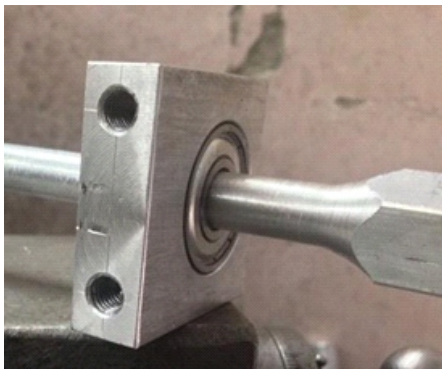

Figure 11. Manufactured bearing mounts

3. EVICES USED FOR TESTING

3.1. Stepper Motor

It was decided to use AC stepper motor in reverse as a generator coupled with the turbine for the experimentation to measure the open circuit voltage and closed circuit current to calculate power by coupling the motor to the output shaft.

Figure 12. Stepper motor with mounted pulley and wiring to measure V-

3.2. Flow Meter

A digital flow meter was setup 30cm ahead of the turbine to calculate the flow velocity of water incident on the blades. Data was logged directly on the laptop by interfacing the meter with Arduino UNO board and running the code to measure the flow velocity. Water flow sensor is mainly consisting of plastic valve body, rotor assembly and Hall Current Sensor. It is installed in the water inlet end for detecting water flow. When water passes through the flow rotor assembly, Magnetic rotor will rotate and Speed will change as the flow

changes. Hall Current sensor provides an output of the corresponding pulse Signal, which is used for calculations.

Figure 13. Flowmeter to measure water velocity

3.3. Tachometer

The RPM at the driven pulley is estimated through a digital tachometer.

3.4. Bearings

Waterproof bearing were purchased according to the bearing load calculations. The FOS of the bearing available for 12mm shafts is more than suffice for the experiment.

3.5. Belt

Rubber belt was selected with minimum width and appropriate load capacity.

3.6. Multi-Meter

The experimental power output is calculated by measuring the current and voltage output at the output terminals of the stepper motor which is being used in reverse as a generator.

4. ASSEMBLED MODEL

The following is the assembled model of the blade-hub assembly along with the flowmeter, arduino, shaft, pulley, belt and stepper motor along with connections for voltmeter. The test bed has gates on both sides whose openings can be varied to regulate the flow velocity and depth of the channel.

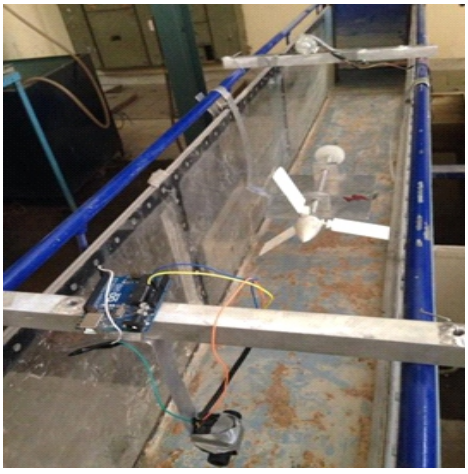

Figure 14. Assembled model of the turbine blades with hub, bearing mounts and shaft.

5. CONCLUSION

The future course of action in this project would be to overcome the challenges of stagnant flow conditions in the upper half of the channel depth due to backpressure from the gates. This assembly when tested in a flow bed with velocity closer to 2m/s is expected to give 15-20W of power which is considerable keeping in mind the dimensions and requirements of the model.

A turbine placed in natural conditions with a flow velocity of 2m/s and radius as 2m would have its power output in the range of 7-8KW which is a sizeable amount of clean and decentralized power with little investment and upkeep. These turbines present a viable solution to the energy problems of the country and are in line to offer an exciting alternative for the country's plan to develop 225GW of clean energy by 2022.

6. REFERENCES

[1]http://www.bp.com/en/global/corporate/energy-economics/statistical-review-of-world-energy/country-and-regional-insights/india-insights.htm

[2] http://www.eia.gov/forecasts/aeo/pdf/electricity_gener ation.pdf; Annual Energy Outlook 2014.

[3]http://www.cea.nic.in/reports/monthly/inst_capacit y/jul15.pdf. Central Electricity Authority, Ministry of Power, Government of India. July 2015. Retrieved 15 Sep 2015.

[4]http://www.cleanenergyactionproject.com/CleanEn ergy Action Project / Hydropower_Case_Studies _files/St rangeford%20Narrows%20SeaGen%20Tidal%20Pow er%20Plant.pdf Strangford Narrows SeaGen Tidal Power Plant, Fundamentals of Renewable Energy, as accessed on October 21, 2015.

[5] Douglas, C.A., G.P. Harrison, and J.P. Chick, Lifecycle assessment of the Seagen marine current turbine. Proceedings of the Institution of MechanicalEngineers Part M: Journal of Engineering for the Maritime Environment, 2008.

[6] http://www.marineturbines.com/SeaGen-Technology/Energy-Capture, official website of Marine Current Turbine Limited, as accessed on October 24, 2015.

[7] Røkke, Astrid, Nilssen, Robert, Marine Current Turbines and Generator preference. A technology review, International Conference on Renewable Energies and Power Quality (ICREPQ'13) Bilbao Spain), 20th to 22th March, 2013.

[8] SeaGen Environmental Monitoring Programme Final Report, as available on http://seageneration.co.uk/files/SeaGen-Envir onmental-Monitoring-Programme-Final-Report.pdf, accessed on October 24, 2015.

[9] Colby, Jonathan. Multi-scale Hydro dynamic analysis of kinetic hydropower arrays. Nortek USA Technical Symposium, March 17, 2011.

[10] Verdant Power, Inc, Final Report - GO18168 Improved Structure and Fabrication of Large, High-Power KHPS Rotors, Award No. DE-FG36-08GO18168.

[11] D. Sale, J. Jonkman, W. Musial; "A Hydrodynamic Optimization Method and Design Code for Stall-Regulated Hydrokinetic Turbine Rotors," OMAE2009; May/June 2009.

[12] Vauthier, Philippe. The underwater electric kite. East river deployment, UEK Corporation.

[13] Nigam, S. Et al, "Design and Pitch Angle optimisation of Horizontal Axis Hydrokinetic Turbine with constant Tip Speed Ratio", 5th ICAME,Singapore 2016.

Instructions for Authors

Essentials for Publishing in this Journal

1 Submitted articles should not have been previously published or be currently under consideration for publication elsewhere.

2 Conference papers may only be submitted if the paper has been completely re-written (taken to mean more than 50%) and the author has cleared any necessary permission with the copyright owner if it has been previously copyrighted.

3 All our articles are refereed through a double-blind process.

4 All authors must declare they have read and agreed to the content of the submitted article and must sign a declaration correspond to the originality of the article.

Submission Process

All articles for this journal must be submitted using our online submissions system. http://enrichedpub.com/ . Please use the Submit Your Article link in the Author Service area.

Manuscript Guidelines

The instructions to authors about the article preparation for publication in the Manuscripts are submitted online, through the e-Ur (Electronic editing) system, developed by **Enriched Publications Pvt. Ltd**. The article should contain the abstract with keywords, introduction, body, conclusion, references and the summary in English language (without heading and subheading enumeration). The article length should not exceed 16 pages of A4 paper format.

Title

The title should be informative. It is in both Journal's and author's best interest to use terms suitable. For indexing and word search. If there are no such terms in the title, the author is strongly advised to add a subtitle. The title should be given in English as well. The titles precede the abstract and the summary in an appropriate language.

Letterhead Title

The letterhead title is given at a top of each page for easier identification of article copies in an Electronic form in particular. It contains the author's surname and first name initial .article title, journal title and collation (year, volume, and issue, first and last page). The journal and article titles can be given in a shortened form.

Author's Name

Full name(s) of author(s) should be used. It is advisable to give the middle initial. Names are given in their original form.

Contact Details

The postal address or the e-mail address of the author (usually of the first one if there are more Authors) is given in the footnote at the bottom of the first page.

Type of Articles

Classification of articles is a duty of the editorial staff and is of special importance. Referees and the members of the editorial staff, or section editors, can propose a category, but the editor-in-chief has the sole responsibility for their classification. Journal articles are classified as follows:

Scientific articles:

1. Original scientific paper (giving the previously unpublished results of the author's own research based on management methods).
2. Survey paper (giving an original, detailed and critical view of a research problem or an area to which the author has made a contribution visible through his self-citation);
3. Short or preliminary communication (original management paper of full format but of a smaller extent or of a preliminary character);
4. Scientific critique or forum (discussion on a particular scientific topic, based exclusively on management argumentation) and commentaries. Exceptionally, in particular areas, a scientific paper in the Journal can be in a form of a monograph or a critical edition of scientific data (historical, archival, lexicographic, bibliographic, data survey, etc.) which were unknown or hardly accessible for scientific research.

Professional articles:

1. Professional paper (contribution offering experience useful for improvement of professional practice but not necessarily based on scientific methods);
2. Informative contribution (editorial, commentary, etc.);
3. Review (of a book, software, case study, scientific event, etc.)

Language

The article should be in English. The grammar and style of the article should be of good quality. The systematized text should be without abbreviations (except standard ones). All measurements must be in SI units. The sequence of formulae is denoted in Arabic numerals in parentheses on the right-hand side.

Abstract and Summary

An abstract is a concise informative presentation of the article content for fast and accurate Evaluation of its relevance. It is both in the Editorial Office's and the author's best interest for an abstract to contain terms often used for indexing and article search. The abstract describes the purpose of the study and the methods, outlines the findings and state the conclusions. A 100- to 250-Word abstract should be placed between the title and the keywords with the body text to follow. Besides an abstract are advised to have a summary in English, at the end of the article, after the Reference list. The summary should be structured and long up to 1/10 of the article length (it is more extensive than the abstract).

Keywords

Keywords are terms or phrases showing adequately the article content for indexing and search purposes. They should be allocated heaving in mind widely accepted international sources (index, dictionary or thesaurus), such as the Web of Science keyword list for science in general. The higher their usage frequency is the better. Up to 10 keywords immediately follow the abstract and the summary, in respective languages.

Acknowledgements

The name and the number of the project or programmed within which the article was realized is given in a separate note at the bottom of the first page together with the name of the institution which financially supported the project or programmed.

Tables and Illustrations

All the captions should be in the original language as well as in English, together with the texts in illustrations if possible. Tables are typed in the same style as the text and are denoted by numerals at the top. Photographs and drawings, placed appropriately in the text, should be clear, precise and suitable for reproduction. Drawings should be created in Word or Corel.

Citation in the Text

Citation in the text must be uniform. When citing references in the text, use the reference number set in square brackets from the Reference list at the end of the article.

Footnotes

Footnotes are given at the bottom of the page with the text they refer to. They can contain less relevant details, additional explanations or used sources (e.g. scientific material, manuals). They cannot replace the cited literature.
The article should be accompanied with a cover letter with the information about the author(s): surname, middle initial, first name, and citizen personal number, rank, title, e-mail address, and affiliation address, home address including municipality, phone number in the office and at home (or a mobile phone number). The cover letter should state the type of the article and tell which illustrations are original and which are not.

Address of the Editorial Office:

Enriched Publications Pvt. Ltd.
S-9,IInd FLOOR, MLU POCKET,
MANISH ABHINAV PLAZA-II, ABOVE FEDERAL BANK,
PLOT NO-5, SECTOR -5, DWARKA, NEW DELHI, INDIA-110075,
PHONE: - + (91)-(11)-45525005